AD-A134 227 ON THE IMPLICATIONS FOR LEFM (LINEAR ELASTIC FRACTURE MECHANICS) OF THE T..(U) CARNEGIE INST OF TECH PITTSBURGH PA DEPT OF MECHANICAL ENGINE.. 1/1

UNCLASSIFIED W S BURTON ET AL. JUN 83 SM-83-8 F/G 20/11 NL

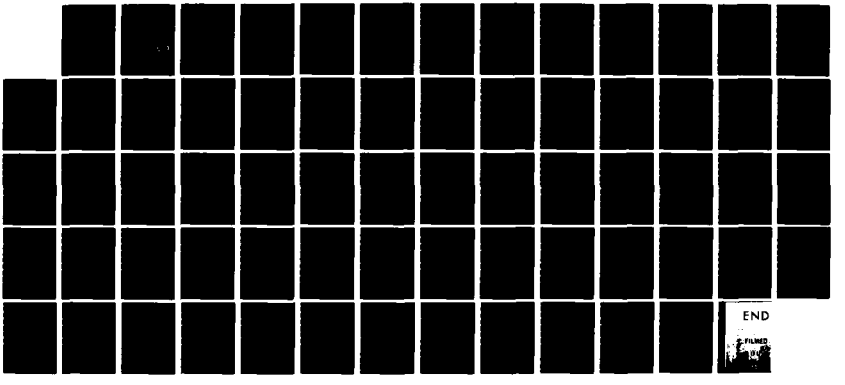

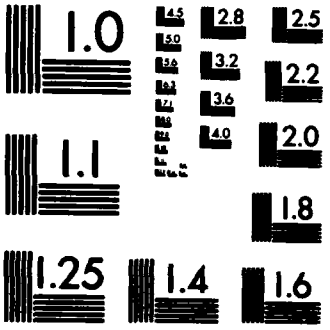

MICROCOPY RESOLUTION TEST CHART
NATIONAL BUREAU OF STANDARDS-1963-A

UNCLASSIFIED

SECURITY CLASSIFICATION OF THIS PAGE (When Data Entered)

13

REPORT DOCUMENTATION PAGE		READ INSTRUCTIONS BEFORE COMPLETING FORM
1. REPORT NUMBER **AFOSR-TR- 83-0863**	2. GOVT ACCESSION NO.	3. RECIPIENT'S CATALOG NUMBER
4. TITLE (and Subtitle) ON THE IMPLICATIONS FOR LEFM OF THE THREE-DIMENSIONAL ASPECTS IN SOME CRACK/SURFACE INTERSECTION PROBLEMS		5. TYPE OF REPORT & PERIOD COVERED FINAL: 01 JUN 79-30 NOV 82
		6. PERFORMING ORG. REPORT NUMBER SM 83-8
7. AUTHOR(s) W S BURTON J L SWEDLOW G B SINCLAIR J B SOLECKI		8. CONTRACT OR GRANT NUMBER(s) AFOSR-79-0078
9. PERFORMING ORGANIZATION NAME AND ADDRESS Department of Mechanical Engineering Carnegie-Mellon University Pittsburhg, PA 15213		10. PROGRAM ELEMENT, PROJECT, TASK AREA & WORK UNIT NUMBERS 61102F 2307/B2
11. CONTROLLING OFFICE NAME AND ADDRESS AFOSR/NA Bolling AFB DC 20332		12. REPORT DATE June 1983
		13. NUMBER OF PAGES 65
14. MONITORING AGENCY NAME & ADDRESS(if different from Controlling Office)		15. SECURITY CLASS. (of this report) UNCLASSIFIED
		15a. DECLASSIFICATION/DOWNGRADING SCHEDULE

AD-A134 227

16. DISTRIBUTION STATEMENT (of this Report)

Approved for public release; distribution unlimited.

17. DISTRIBUTION STATEMENT (of the abstract entered in Block 20, if different from Report)

DTIC ELECTE OCT 31 1983 S D E

18. SUPPLEMENTARY NOTES

DTIC FILE COPY

19. KEY WORDS (Continue on reverse side if necessary and identify by block number)

THREE-DIMENSIONAL CRACKS
ELASTIC CRACK/SURFACE INTERACTIONS
LINEAR ELASTIC FRACTURE MECHANICS
INTEGRAL EQUATION ANALYSIS
SINGULAR FINITE ELEMENTS

20. ABSTRACT (Continue on reverse side if necessary and identify by block number) Several elastic configurations containing cracks under transverse tension which intersect a free surface are investigated. In order to ensure reliable results two independent numerical methods are employed on a comparison problem, each method being tuned to handle the special features involved. The comparison provides confidence in other results which focus on the key quantity in linear elastic fracture mechanics, the energy release rate. These findings may be summarized as follows: that the decays in the energy release rates found as the free surface is

DD FORM 1 JAN 73 1473 EDITION OF 1 NOV 65 IS OBSOLETE

UNCLASSIFIED

SECURITY CLASSIFICATION OF THIS PAGE (When Data Entered)

approached in the various problems treated are probably not significant from a fracture toughness testing point of view and not of major consequence in cyclic life calculations, although there are some indications that this may not be the case if near-surface residual stress fields are present; and that these variations in energy release rate can be compensated for by relatively minor perturbations in crack-front profiles.

ON THE IMPLICATIONS FOR LEFM OF THE THREE-DIMENSIONAL ASPECTS IN SOME CRACK/SURFACE INTERSECTION PROBLEMS

FINAL SCIENTIFIC REPORT ON AFOSR-79-0078

W.S. Burton, G.B. Sinclair, J.S. Solecki and J.L. Swedlow

Report SM 83-8 June, 1983

Department of Mechanical Engineering
Carnegie Institute of Technology
Carnegie-Mellon University
Pittsburgh, Pennsylvania

Table of contents

Preface

The original research proposal, from which the work reported here is an outcome, had as its objectives:

- The general quantification and understanding of the import for linear elastic fracture mechanics of three-dimensional effects in crack/surface intersection configurations, and in particular the determination of associated crack profiles that are critical in an LEFM sense.
- The development of two independent numerical approaches for the attendant analysis, both of which to be sufficiently well adapted to the class of problems of concern so as to have high resolution; the two methods to be used jointly initially so as to provide mutual confirmation but ultimately being used separately to each's respective greatest effectiveness.

The extent to which the first objective has been met is summarized in the abstract that follows immediately and described with greater detail and commentary in the last of Section 4 and Section 5. The extent to which the second objective has been fulfilled is apparent from Section 3, the first part of Section 4 and the last AFOSR technical report filed. Both activities are placed in perspective with other related contributions to the literature in the review in Section 1. In sum, these various sources evidence a significant degree of success in achieving the basic aims of the research program.

Abstract

Several elastic configurations containing cracks under transverse tension which intersect a free surface are investigated. In order to ensure reliable results two independent numerical methods are employed on a comparison problem, each method being tuned to handle the special features involved. The comparison provides confidence in other results which focus on the key quantity in linear elastic fracture mechanics, the energy release rate. These findings may be summarized as follows: that the decays in the energy release rates found as the free surface is approached in the various problems treated are probably not significant from a fracture toughness testing point of view and not of major consequence in cyclic life calculations, although there are some indications that this may not be the case if near-surface residual stress fields are present; and that these variations in energy release rate can be compensated for by relatively minor perturbations in crack-front profiles.

1. Introduction

During the past twenty-five years *linear elastic fracture mechanics* (LEFM) has emerged as the technology whereby the engineer predicts fast fracture in brittle instances and tracks cyclic crack growth even in some ductile materials. The basis of this technology lies in the identification of the classical singular stresses and strains that occur at a crack tip in plane elasticity, followed by an integration of these unrealistic fields to form a physically meaningful, *energy release rate*, or crack driving energy, G: then unstable crack propagation is predicted when G attains a critical material value, and fatigue crack growth under cyclic loading can be estimated using a data reduction scheme based in essence on the oscillation in $\sqrt{G}$, $\Delta\sqrt{G}$.* While the approach within its limitations is well understood in two dimensions it is less so in three. Moreover configurations occur quite often in practice that are inherently *three-dimensional*; for example, the intersection of a crack with a surface, especially in the presence of shallow residual stress distributions. Our objective here is to further the understanding of the importance of such three-dimensional features within the context of LEFM.

Specifically we focus attention on *cracks under transverse loading that intersect free surfaces* because of their potentially major implications in engineering, and seek an appreciation of associated three-dimensional (3-D) effects on the all-important energy release rate. Thus we need to identify the local singular character present in these 3-D situations and, since G can no longer be taken as being constant along the crack front, to assess

*Both of these predictive tools are more usually couched in terms of a stress intensity factor K and its fluctuation under cyclic loading ΔK: nonetheless the physical reasoning underlying the approach remains that of an energy balance and K's significance stems from its equivalence to G.

its variation there. In fact the LEFM postulates of a critical value for G for fast fracture and of $\Delta\sqrt{G}$ governing fatigue crack growth insist that, in 3-D configurations, we look for crack-front profiles having a constant G if they are to be everywhere *critical* or a constant $\Delta\sqrt{G}$ if they are to be associated with steady *self-similar* crack growth. That is, we need to solve free boundary value problems to determine the shapes of the crack fronts. The consideration of these issues is the major concern of this paper.

Over the years a large number of contributions to the LEFM literature which address various aspects of the influence of three-dimensionality have been made - see Panasyuk, Andrejkiv and Stadnik [1], [2] for reviews through 1981 which together cite some 500 odd related references. In commenting on the impact of these investigations on the issues of interest here, we begin with attempts to elucidate local singular nature which are primarily analytical, then turn to numerical treatments of more global problems.

To fix ideas in our initial commentary we consider a generic configuration entailing the normal intersection of a free surface by a crack under transverse tension (Fig. 1). If R denotes this cracked elastic region we have, on introducing spherical polar coordinates (ρ,θ,ϕ) with origin 0 at the crack/surface intersection or crack vertex,

$$R = \{(\rho,\theta,\phi) \mid 0 \leq \rho < \infty,\ 0 \leq \theta \leq \pi/2,\ 0 < \phi < 2\pi\}. \tag{1}$$

To aid the exposition further we also introduce cylindrical polar coordinates (r,ϕ,z) sharing the same origin and related to (ρ,θ,ϕ) by

$$r = \rho\sin\theta,\ \phi = \phi,\ z = \rho\cos\theta, \tag{2}$$

on R. The key question pertaining to this configuration is what are the possible *singular* aspects of the elastic stresses near the crack front in the vicinity of 0, *viz.*, as $\rho \to 0$ or as $r,\ z \to 0$.

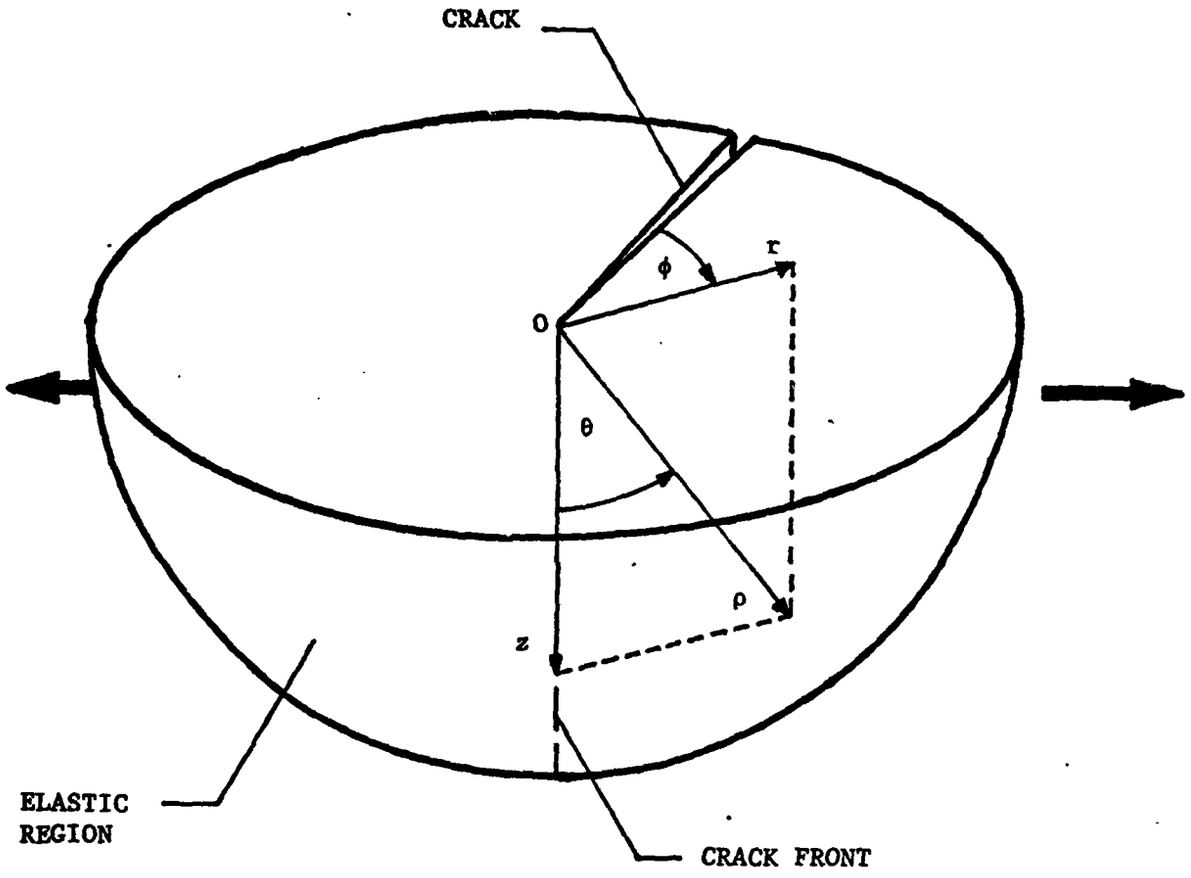

Figure 1. Coordinates for generic 3-D crack configuration.

To address this question we first draw on the work of Aksentian [3] which expands the three-dimensional equations of elasticity in local curvilinear coordinates to establish that the stress behavior anywhere along the crack front in R, except right in the upper plane ($\theta = \pi/2$ or $z = 0$), is governed by the same eigenvalue equation as that derived by Williams [4] for the two-dimensional case. Thus for this part of the crack front we have the classical inverse square-root singularity,

$$\sigma = O(1/\sqrt{r}) \text{ as } r \to 0 \ (z > 0), \tag{3}$$

on R. Of course there is an infinity of other eigenvalues giving rise to eigenfunctions with stronger singularities than that of (3) which are acceptable *local* solutions.* Although these singularities are usually disregarded on the grounds that they lead to unbounded displacements, the dislike of such physically unrealistic displacement responses does not really constitute an argument for their exclusion in any completely formulated *global* problem - after all, the stresses admitted in (3) are certainly not physically appealing even though their displacements are finite. A real reason prohibiting these more singular stresses is that there are associated forces on plane regions of *finite* extent ahead of the crack that are *infinite*, so that, provided we agree *not* to load any finite surface within R with an infinite force, equilibrium insists that they do not participate. Physically, it would be better still if one could argue against the participation of the classical singular stresses too. Rather though, the absence of any two-dimensional eigenfunction which transmits a *transverse tensile stress* ahead of the crack, and does not vanish as $r \to 0$, ensures that the singularity in (3) is always excited in the two-dimensional setting

*Acceptable local solutions in the sense that they satisfy the field equations and the local homogeneous boundary conditions.

when the crack is pulled apart and means we can therefore expect its participation in any like three-dimensional situation. Fortunately it is precisely this singular nature which can result in a positive, finite, energy release rate so that the behavior in (3) is quite acceptable from an LEFM point of view.

It remains to consider, for our generic 3-D crack configuration, the singular character actually in the upper plane. Three analyses which investigate this are Benthem [5], Kawai, Fujitani and Kumagai [6], and Sinclair [7]. All three model their approach to some degree on Williams' separable eigenfunction analysis [4], Benthem [5] using spherical coordinates and satisfying the stress-free conditions on the crack faces exactly, the stress-free conditions on the upper surface approximately; Kawai *et al.* [6] using the same coordinates but satisfying the crack-face conditions approximately, the upper surface conditions exactly; and Sinclair [7] using cylindrical coordinates and meeting the boundary conditions in a similar way to Benthem [5]. All three confirm the classical singular nature away from the upper surface, as in (3). All three recover the one known stress singularity for a Poisson's ratio ν of zero - the value such that two-dimensional solutions completely comply with the local three-dimensional requirements - though Kawai *et al.* [6] indicate the possibility of a stronger singularity as well for this case. And, aside from this last, all three have qualitatively similar behavior as the free surface is approached with

$$\sigma = O(\rho^{\lambda}/\sqrt{r}) \text{ as } r \to 0, \tag{4}$$

on R in Benthem [5], Kawai *et al.* [6], the exponent λ varying from 0 to 0.17, 0 to 0.32 in [5], [6] respectively, as ν ranges from 0 to 0.5, while

$$\sigma = O(z^{2n}/\sqrt{r}) \text{ as } r \to 0, \; n = 1, 2, \ldots, \tag{5}$$

on R in Sinclair [7], for $\nu \neq 0$. No completeness argument for any of the above analyses is apparently available and in fact their difference in detail may well be due to a lack thereof.* Nonetheless, in sum it would seem reasonable to expect behavior like that of (3), (4), (5) to be found in any 3-D problem which becomes two-dimensional when Poisson's ratio is zero, and accordingly to expect a bounded energy release rate which is positive except right in the upper free surface.

A related analytical treatment which contains the local geometry of Fig. 1, yet attempts the ambitious task of the closed form solution to a truly three-dimensional, global, crack problem, is furnished by Folias in [9] and has generated some controversy - see discussion by Benthem and Koiter and author's closure [10]. The main source of contention is the appearance in Folias [9] of the following dominant singular behavior in the normal stress component σ_z:

$$\sigma_z = \frac{k \cos\theta \cos(2\nu+1)\theta}{\rho^{2\nu}\sqrt{\rho\sin\theta}} \cos\frac{\phi}{2} + \ldots \text{ as } \rho \to 0, \qquad (6)$$

where k is a constant ($k \neq 0$). This singularity is stronger than (4), (5) and for $\nu > 1/4$ gives rise to unbounded displacements. As pointed out earlier, while such displacements are perhaps physically counter-intuitive, they are not in themselves a mathematical objection to the validity of the elasticity solution in Folias [9], but rather raise the possibility that, given the loading in [9], the stress in (6) does not meet equilibrium requirements. Indeed inspection of (6) shows this to be so, since equilibrium in the z-direction at the *free* surface ($\theta = \pi/2$) requires $\partial/\partial z$ of σ_z to be null there (equivalently $\partial\sigma_z/\partial\theta$ to be zero), and it is *not* (for $\nu \neq 0$). Of course

*It might appear that the two-dimensional completeness proof of Gregory [8], via Aksentian's argument [4], applies here for $z > 0$; unfortunately an additional separation-of-variables assumption is necessary in [4] so that completeness remains unproven even away from $z = 0$ for $\nu \neq 0$.

the method of solution construction adopted by Folias in [9] assures satisfaction of the equilibrium requirements by his stress fields *in toto*, so there must be further contributions to the stress field in [9], not to date explicitly extracted, which combine with σ_z of (6) to restore this compliance and in doing so may even annihilate it! We conclude therefore that the singularity present at the crack/surface intersection in Folias' problem [9] is still to be determined and consequently our expectations as to the behavior there remain unaltered by [9].

The investigations [5], [6], [7], [9] do have one thing in common - they all attest to the difficulty of constructing analytical solutions for 3-D cracks and it seems almost certain that the more complex configurations of concern here are intractable to purely analytical approaches. As a result we look to numerical methods and next review the accompanying literature, starting with those contributions that are most closely connected to the aforementioned analytical studies.

The local eigenvalue problem indicated in Fig. 1, with geometry as in (1) if $\rho \leq 1$ therein, is analyzed in Benthem [11] via *finite differences* and the eigenvalues in Benthem's earlier paper [5] confirmed, the maximum discrepancy between the two determinations occuring when $\nu = 1/2$ and being only 4%. Unfortunately the numerical approach in [11] does not readily admit to more general application and probably the most obvious candidate towards this end is the *finite element method* (FEM). Bažant and Estenssoro [12] use a version of the finite element method on the same local geometry as in Benthem [11]. The most distinctive aspect of the FEM in Bažant and Estenssoro [12] is the representation of the fields near the crack vertex with expressions which contain an adjustable exponent governing the singularity there, the exponent being estimated by a variational

principle - an idea developed independently and somewhat differently by Bažant [13] and Swedlow [14], [15]. Using a sequence of grids, Bažant and Extenssoro [12] demonstrate convergence and, by extrapolating their results, also confirm Benthem's values for the singular eigenvalue [5]. As a consequence of the representations *assumed* in Bažant and Estenssoro [12], this confirmation does not constitute a completeness argument for Benthem's forms in [5] but it is quite reassuring as regards our expectations of singular behavior, hence G, in this critical region. In addition in Bažant and Estenssorc [12] , intersection other than normal is considered and angles found at which the singularity exponent becomes 1/2 ($\lambda = 0$ in (4)), thus angles of intersection for a straight inclined crack for which positive energy release rates may exist right in the upper surface.

The success enjoyed by these *local* numerical analyses is not found to the same extent in finite element treatments of more *global* or *complete* problems which contain crack/surface intersections, although some worthwhile attempts have been recently reported: see Yamamoto and Sumi [16], Yagawa and Nishioka [17], [18] which use superposition; Raju and Newman [19], Sebra Pereira [20], Tseng [21], Hilton and Kiefer [22] which use special elements.* Two requirements for reliable results in this sort of analysis are that the crack-tip representations of field quantities be able to model both singular and regular behavior while retaining compatibility with the fields away from the crack-tip, and that any quadrature scheme used should recognize the singular representation adequately. To varying degrees the investigations in [16] - [22] meet these requirements. However, all of these papers have to *assume* singular

*This list is not intended to be comprehensive but merely representative of the better finite element solutions for the class of complete, elastic, 3D crack problems considered here: we are not aware, though, of any other markedly superior FEM analysis for a problem of this type.

character *a priori* and, presumably because of the size of the computational task involved in global three-dimensional geometries, none manage to carry out the calculations on a sufficiently refined sequence of grids so as to establish *numerical convergence* - an essential demonstration in view of the possibility of an inappropriate assumption as to singular character, and in view of the different predictions concerning the variation in the energy release rate in [16] - [22] with some results showing an increase in G in the near surface, some a decrease, and still others no change. It would seem therefore that, in the global situation, a numerical approach with a higher analytical component might be advisable if computational efficiency is to attain levels that enable convergence to be checked.

A more analytical procedure is the *method of lines* which integrates displacements exactly in their own directions and uses finite difference approximations for their gradients in transverse directions. Application of the method to global configurations containing cracks with normal intersections of free surfaces is described in Gyekenysei and Mendelson [23]. In [23] G can be inferred to remain constant or to increase as the free surface is approached depending on overall specimen geometry, clearly a contradiction to the expectation expressed in (4), (5). What is not clear in Gyekenysei and Mendelson [23] is how well the singularities in the displacement derivatives are approximated by the finite differences, so that there is some doubt as to the reliability of the results obtained by means of this method at this time.

Another more analytical approach than FEM is the *boundary integral equation method* (BIE) which employs a Green's function to meet the field equations exactly, thus reducing the problem to boundary condition satisfaction on surfaces; *i.e.*, the region to be discretized for numerics is reduced from three dimensions in FEM to two dimensions in BIE. An early

use of this method on a complete 3-D crack problem is that by Cruse and Van Buren [24] and remains even today one of the more refined analyses - at least as judged by the size of the discretization regions near the crack. A more recent application of BIE to a problem of this class is that of Tan and Fenner [25] which has a higher order representation of the unknowns involved yet still does not take their singular behavior into account. Both Cruse and Van Buren [24] and Tan and Fenner [25] find evidence of a decay in the energy release rate as the free surface is approached but neither fully confirms their findings with a convergence check on a discretization sequence. In order to do this check, *special integral equations* that exploit a match between a particular Green's function and a restricted class of three-dimensional crack geometries may prove advantageous. Recently two such integral equation sets have been derived by Folias [26] and Smetanin and Sobol [27]; currently though no results from their numerical analysis seem to be available.

In the light of the preceding, this investigation uses a special set of integral equations developed in Sinclair [28] for an elastic half-space weakened by a crack of finite width and infinite depth subjected to transverse excitation. This integral equation set has a single physical unknown, is more compact than that of Folias [26] but comparable in complexity to that of Smetanin and Sobol [27], and has the attribute of recovering exactly the closed form two-dimensional solution that obtains for the configuration under the simplifying assumptions of normal intersection, uniform far-field tension and a Poisson's ratio of zero. Furthermore, the singular nature of the unknown in the set needs only to be dominated, not estimated precisely, to ensure convergence, and this last concern is examined on a sequence of three discretizations, the finest of which provides information at distances in advance of the crack front which are about a factor of four closer than

the closest in Cruse and Van Buren [24]. On the other hand, little is learned of the precise singular behavior in the crack vertex proximity from the system. To compensate we also employ a finite element method to analyse a finite geometry of sufficiently gross dimensions so as to simulate the half-space implicitly required in our integral equation development. The FEM features an adjustable singularity exponent at the crack vertex (after Bažant and Estenssoro [12], Swedlow [15]) so that the singularity there is not completely assumed in advance; further the special crack-tip elements involved also contain regular fields and are compatible with host elements, and singular quadrature is used. By comparison with the integral equation results its convergence can be inferred. With the two numerical approaches thus verified they can then be used to each's best advantage to study critical crack profiles, residual stress effects, and the influence of plate thickness.

We begin in Section 2 by stating the 3-D problems for analysis via the integral equation and finite element approaches. In Section 3 we describe the analysis, commencing with the derivation and numerics associated with the integral equations, and closing with the development of the FEM. In Section 4 we present results obtained, commencing with those which serve to validate the overall treatment, and closing with those which quantify selected three-dimensional effects in LEFM. Finally in Section 5 we offer some concluding remarks.

2. Formulation of three-dimensional problems

Here we consider two companion geometries for the examination of the three-dimensional aspects of crack/surface interactions. The first is an infinite geometry chosen with a view to facilitating integral equation development,

the second a finite geometry designed to enable comparison of an FEM treatment. We start with a formal statement of the simplest problem analyzed via integral equations and continue with a discussion of some generalizations of this configuration to address other issues of physical importance. We then follow the same pattern in describing the problems for finite element analysis.

One configuration amenable to *integral equation* development is that of an elastic half-space, containing a crack of finite width and infinite depth, under uniform transverse tension at infinity σ_y° (Fig. 2). This choice is not uniquely well suited to our present purpose but is sensible in that it has a characteristic length, is subjected to opening (Mode I) excitation, and does enable a compact set of integral equations to be subsequently derived in the next section. With the development of the integral equation system in mind we subtract a uniform transverse tension of magnitude σ_y° throughout an *uncracked* half-space to recover a configuration wherein the crack is opened by a constant normal pressure equal to σ_y°, then exploit the symmetry about the crack plane to formulate the problem in rectangular cartesian coordinates (x,y,z) on the quarter space $\mathcal{Q}$,

$$\mathcal{Q} = \{(x,y,z) \mid -\infty < x < \infty,\ 0 < y < \infty,\ 0 < z < \infty\}. \tag{7}$$

For this quarter-space we denote the upper surface by $\partial_1\mathcal{Q}$ and the surfaces corresponding to the crack face and the connected material in the crack plane by $\partial_2\mathcal{Q}$, $\partial_3\mathcal{Q}$ respectively. Thus

$$\begin{aligned}
\partial_1\mathcal{Q} &= \{(x,y,z) \mid -\infty < x < \infty,\ 0 < y < \infty,\ z = 0\},\\
\partial_2\mathcal{Q} &= \{(x,y,z) \mid 0 < |x| < a,\ y = 0,\ 0 < z < \infty\},\\
\partial_3\mathcal{Q} &= \{(x,y,z) \mid a < |x| < \infty,\ y = 0,\ 0 < z < \infty\},
\end{aligned} \tag{8}$$

wherein a is the semi-crack length. We seek then, in general, the stresses σ_x, σ_y, σ_z, τ_{xy}, τ_{yz}, τ_{zx} and displacements u, v, w as functions of x, y, z

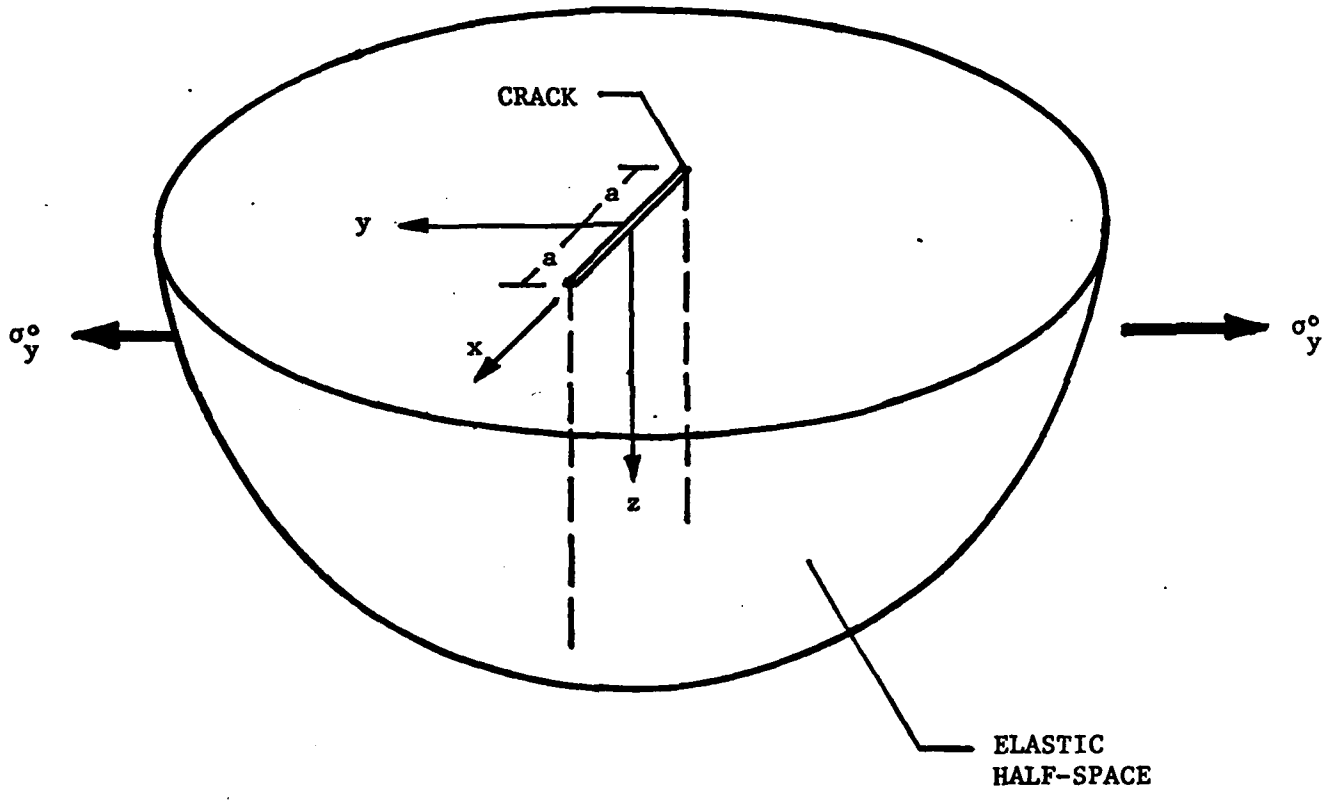

Figure 2. Coordinates for the basic infinite configuration.

throughout $\mathcal{Q}$, satisfying: the three-dimensional stress equations of equilibrium in the absence of body forces, on $\mathcal{Q}$; the stress-displacement relations for a homogeneous, isotropic and linear elastic continuum with shear modulus μ and Poisson's ratio ν, throughout $\mathcal{Q}$;* the stress-free conditions on the upper surface,

$$\sigma_z = \tau_{yz} = \tau_{zx} = 0, \tag{9}$$

on $\partial_1\mathcal{Q}$; the opening-pressure stress conditions on the crack face,

$$\sigma_y = -\sigma_y^\circ \ , \ \tau_{xy} = \tau_{yz} = 0, \tag{10}$$

on $\partial_2\mathcal{Q}$; the symmetry conditions ahead of the crack,

$$\tau_{xy} = \tau_{yz} = 0, \ v = 0, \tag{11}$$

on $\partial_3\mathcal{Q}$; and finally the conditions at infinity which insist that the stresses approach a plane strain state for a crack opened under constant pressure,

$$\begin{aligned} &\sigma_x = o(1), \ \tau_{xy} = o(1), \ \tau_{xz} = o(1) \text{ as } x^2 \to \infty, \\ &\sigma_y = o(1), \ \tau_{xy} = o(1), \ \tau_{yz} = o(1) \text{ as } y \to \infty, \\ &\sigma_z = \sigma_z^p + o(1), \ \tau_{yz} = o(1), \ \tau_{zx} = o(1) \text{ as } z \to \infty, \end{aligned} \tag{12}$$

on $\mathcal{Q}$, where σ_z^p is the plane strain, out-of-plane, normal stress (refer, for instance, Green and Zerna [30], §8.17 for details),

$$\sigma_z^p = 2\nu \, \sigma_y^\circ \left[\frac{r_o}{\sqrt{r_1 r_2}} \cos\left(\phi_o - \frac{\phi_1}{2} - \frac{\phi_2}{2}\right) - 1\right], \tag{13}$$

with

$$r_i = \sqrt{\left[(x + i(5-3i)a/2)^2 + y^2\right]}, \ \phi_i = \sin^{-1}(y/r_i) \ (i = 0,1,2),$$

on $\partial_1\mathcal{Q}$. In particular we wish to draw from the stresses and displacements complying with this formulation the attendant energy release rate and consider three-dimensional effects thereon.

*The usual notation for stresses and displacements is employed; for details of the field equations see, for example, Timoshenko and Goodier [29], pp. 7, 11,236.

The *energy release rate* G here may be represented using any one of several equivalent integral forms. Viewing G as the incipient local work required to heal the direct extension of a crack in the opening mode per unit length of that extension, one such integral is, after Irwin [31],

$$G = \lim_{\delta a \to 0} \frac{1}{\delta a} \int^{a+\delta a} \sigma_y^a \, \delta v dx. \tag{14}$$

Here δa is the extension of the crack in the x-direction through material initially experiencing the tensile stress σ_y^a and δv is the opening displacement accompanying this extension. Implicit in (14) and its equivalent forms is a *requirement on the local singular character* so that the integration yields a finite non-trivial result. The determination of this requisite singular nature proceeds routinely. We take the most singular aspect of the stress distribution σ_y^a along the x-axis to be described by,

$$\sigma_y^a = C_1 \, (x-a)^{\lambda} \, (1 + o(1)) \text{ as } x \to a^+ \, (\lambda > -1), \tag{15}$$

where λ is the exponent characterizing the singularity and C_1 a constant. This in turn implies an associated shifted displacement of

$$\delta v = C_2 (a+\delta a-x)^{\lambda+1} \, (1 + o(1)) \text{ as } x \to (a + \delta a)^-, \tag{16}$$

C_2 a constant. Then introducing the forms (15), (16) into (14) and making the change to the variable $x' = (x-a)/\delta a$ gives

$$G = \lim_{\delta a \to 0} C_1 \, C_2 \, \delta a^{2\lambda+1} \, B(\lambda+1,\lambda+2), \tag{17}$$

where $B(\lambda+1,\lambda+2)$ is the Beta function, bounded for $\lambda > -1$. Equation (17) insists that $\lambda = -\frac{1}{2}$ in order for G to be bounded and positive.

Also implicit in (14) is that in two dimensions G is uniform along the crack front, whereas in three dimensions this integral represents an energy release rate *per unit length of crack front* and its constancy is not

assured. Thus in order that the entire crack front be critical, we cannot assume its shape *a priori* but must determine it such that G is uniform.

Currently two-dimensional testing assumes, in effect, a straight crack front to be critical and on this basis estimates the critical value G_c for fracture, the material property one seeks essentially in fracture toughness testing. On the one hand the attendant curvature restrictions in these tests may result in unnecessarily discarding useful data (as in Kaufman [32]); on the other, the *average* G found via two-dimensional analysis for a straight or nearly straight crack, set equal to G_c at fracture, may be significantly lower than the actual three-dimensional *maximum*, thereby leading to an overly conservative estimate of this critical energy. Now the usual physical situation preceding fracture - cyclic growth up to the point of unstable crack propagation - indicates near uniform advances of curved crack profiles (as in, for example, Bell and Feeney [33]). Thus a more realistic calculation of G_c would result if we considered these fronts, which may reasonably be taken to possess constant energy release rates, and at failure, a constant G_c. In order to state the associated free-boundary problem precisely, we need to choose the plane in which the energy release rate is calculated to best model the observed, approximately, self-similar, crack growth. Here two likely candidates present themselves; normal to the crack front and parallel to the free surface (this last actually being the direction in (14)). To select one of these we consider the consequences of local crack advances governed by a Paris data reduction scheme for cyclic loading. For either direction, beginning with an assumed profile of constant G, the crack under a Paris relation is advanced a uniform increment δa in a single cycle directed in the plane in which G is calculated. We see then (Fig. 3) that only a crack advance associated with G calculated in the plane parallel to the free surface produces a crack that retains its shape. Accordingly, we choose

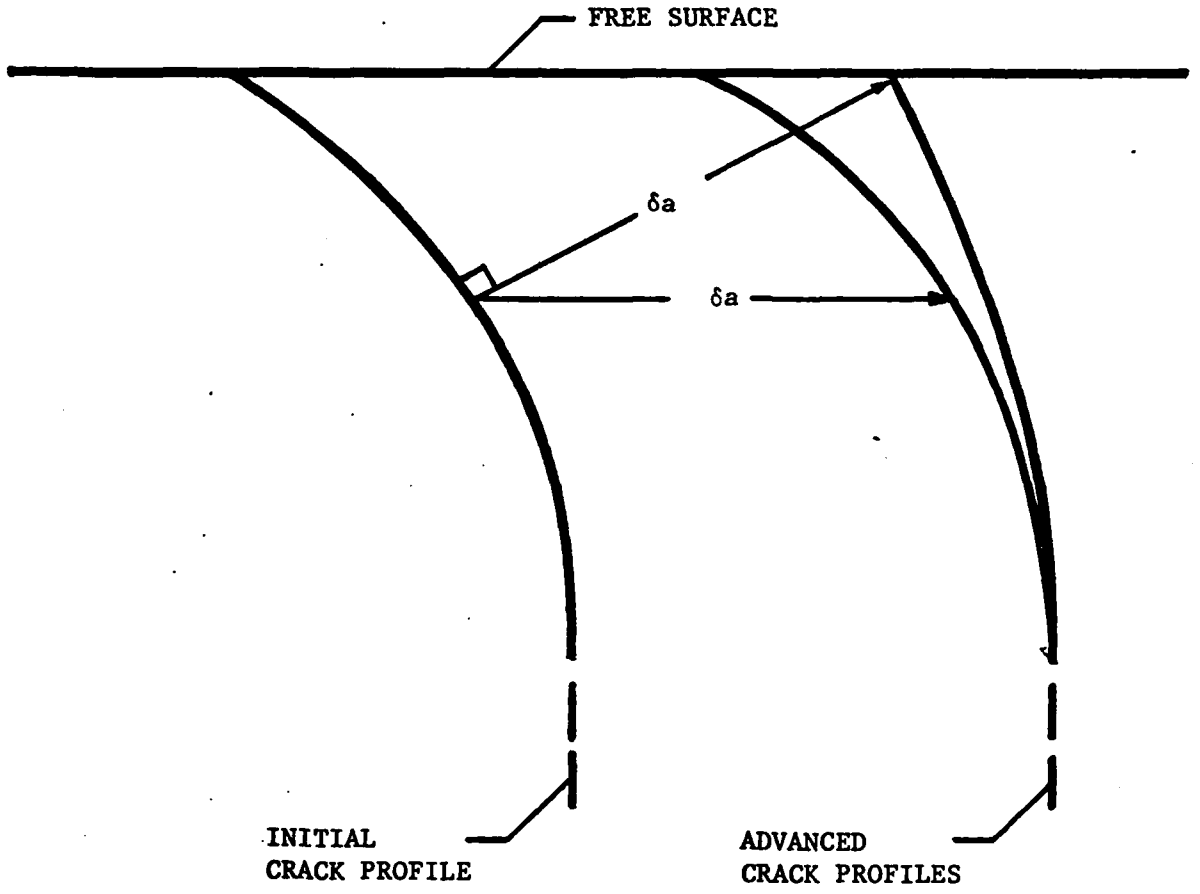

Figure 3. Candidate directions of crack advance to achieve self-similar profiles.

this plane for the calculation of the energy release rate. As a result, the pertinent free boundary problem seeks, in addition to the stresses and displacements satisfying all of our preceding requirements, to determine the crack profile, $a = a(z)$, such that, in light of the singularity requirement demanded by (17), we have,

$$\lim_{x \to a^+} \sigma_y \sqrt{(x - a)} = C_o, \tag{18}$$

on $\partial_3 Q$, C_o being a constant.

Another distinctly three-dimensional problem in LEFM that can be addressed through a generalization of the previous integral equation formulation is the effect on the energy release rate of a crack embedded in a *non-uniform residual stress field*. In practice, one attempts to induce near-surface, compressive, residual stress distributions to inhibit fatigue crack initiation and propagation. It is not intended here to trace the actual physical processes which lead to these distributions, a difficult non-linear elasto-plastic problem, but instead we look to perform a series of numerical experiments to quantify the LEFM implications of some *presumed*, representative, compressive residual stresses. Based on typical experimental results for compressive stresses imposed by a shot peening (see, for example, Almen and Black [34], p. 58), we choose to represent the residual stress field as exponentially decaying away from the free surface. More precisely, we take the residual stress distribution on the crack face to be

$$\sigma_y^r = -C_r e^{-\gamma z/a}, \tag{19}$$

on $\partial_2 Q$, where the magnitude and depth of penetration of this field are governed by the positive constants C_r and γ respectively. The associated problem is as previously stated except that the crack is now opened by the constant

pressure σ_y° minus σ_y^r, *i.e.*, (10) becomes

$$\sigma_y = -\sigma_y^\circ - \sigma_y^r, \ \tau_{xy} = \tau_{yz} = 0, \tag{20}$$

on $\partial_2 Q$. In an attempt to ensure no interpenetration of the opposing crack flanks we make σ_y nowhere positive on $\partial_2 Q$ by setting C_r equal to σ_y°, and examine the effects of different decay rates γ.

Turning to problems to be analyzed via the *FEM* approach, the primary one for comparison requires that we select a *finite* geometry to simulate the baseline integral equation configuration of Fig. 2. Thus we make the finite problem large enough so that the effects of its limited extent are negligible at the crack front. We arrive at the *in-plane* dimensions by considering the two-dimensional analysis of Isida [35] for a center-cracked plate in the opening mode. In [35] a crack length to plate width ratio, a/b, of 1/10 and a plate length to width ratio, c/b, of 2 yields a difference in the singular participation factor of less than one percent from the corresponding two-dimensional infinite plate problem. Hence we take these to be the dimensions here. For the *out-of-plane* dimension, no two-dimensional problem readily enables a similar sizing. We choose a plate thickness to the crack length ratio, h/a, of 2 in an attempt to recover the generalized plane strain solution at the plate midplane; our selection requires subsequent checking to see if this is in fact the case. The resulting geometry is subjected to a uniform uniaxial tensile load σ_y° normal to the crack plane on the plate ends (Fig. 4, not to scale).

Looking to minimize the region to be discretized ultimately in the finite element analysis, we exploit the symmetries about the plate mid-face, the crack plane and the plane normal to and bisecting the crack plane, to formulate the baseline problem in rectangular coordinates (x,y,z) on the plate octant P,

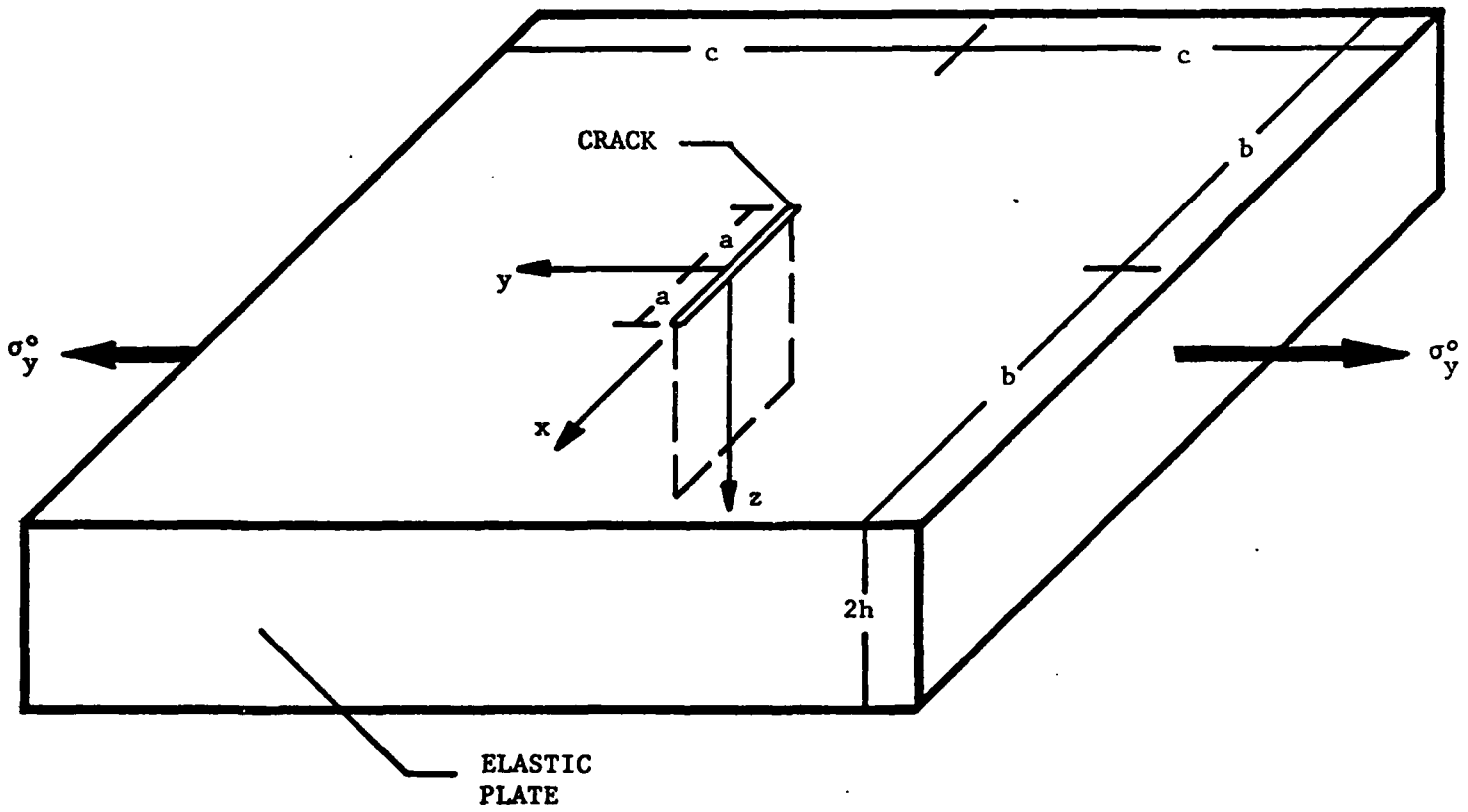

Figure 4. Coordinates for the basic finite configuration.

$$P = \{(x,y,z) \mid 0 < x < b,\ 0 < y < c,\ 0 < z < h\}, \tag{21}$$

having plate upper face $\partial_1 P$ and mid-face $\partial_2 P$ given by

$$\partial_i P = \{(x,y,z) \mid 0 < x < b,\ 0 < y < c,\ z = (i-1)h\}\ (i = 1,2), \tag{22}$$

with mid-plate and outer plate edges $\partial_3 P$, $\partial_4 P$ respectively as in

$$\partial_i P = \{(x,y,z) \mid x = (i-3)b,\ 0 < y < c,\ 0 < z < h\}\ (i = 3,4), \tag{23}$$

and having crack flank $\partial_5 P$, crack plane connecting surface $\partial_6 P$, and plate end $\partial_7 P$ defined by

$$\partial_i P = \{(x,y,z) \mid (i-5)(7-i)a < x < (6-i)(7-i)\frac{(a-b)}{2} + b,\ y = (i-6)(i-5)\frac{c}{2},\ 0 < z < h\}\ (i = 5,6,7). \tag{24}$$

We seek then, in general, the stresses and displacements as functions of x,y,z throughout P satisfying: the same elastic field equations as previously outlined, throughout P; the stress boundary conditions on the loaded end and the free crack flank,

$$\sigma_y = \sigma_y^\circ,\ \tau_{xy} = \tau_{yz} = 0 \quad \text{and} \quad \sigma_y = \tau_{xy} = \tau_{yz} = 0, \tag{25}$$

on $\partial_7 P$, $\partial_5 P$ respectively; the free edge and free face conditions,

$$\sigma_x = \tau_{xy} = \tau_{zx} = 0 \quad \text{and} \quad \sigma_z = \tau_{zx} = \tau_{yz} = 0, \tag{26}$$

on $\partial_4 P$, $\partial_1 P$ respectively; the symmetry conditions on the plate mid-face and the mid-plate edge,

$$\tau_{yz} = \tau_{zx} = 0,\ w = 0 \quad \text{and} \quad \tau_{xy} = \tau_{zx} = 0,\ u = 0, \tag{27}$$

on $\partial_2 P$, $\partial_3 P$ respectively; and the symmetry conditions on the plane ahead of the crack,

$$\tau_{xy} = \tau_{yz} = 0,\ v = 0, \tag{28}$$

on $\partial_6 P$. In particular we wish to extract from the stresses and displacements complying with the above, the energy release rate G as defined in (14).

In the selection of the finite geometry we chose the thickness ratio h/a so as to allow a comparison with the basic infinite problem posed. We cannot make this choice in advance but must consider a succession of problems, where we vary the h/a, until we obtain the desired midplane result. Then, in addition to determining a useful geometry for comparison, we may examine the effects of plate thickness on the crack driving energy along the crack front, that is, the interaction of two crack/surface intersections. With the variation in G quantified, a natural extension of the FEM investigation is a search for critical profiles with a constant G, to wit, profiles meeting (18). This last completes the set of problems we consider.

3. Integral equation and finite element analyses

In this section we establish a set of integral equations for our basic infinite 3-D problem and discuss extensions of the set to accommodate the generalizations of interest. Then we examine the issues entailed in the numerical solution of such integral equation sets. Finally we describe the finite element analysis of the companion finite 3-D problems, paying particular attention to the special features involved in their treatment.

To improve the *convergence* of the integrals in our integral equations, we start by modifying the basic infinite problem by removing the plane strain solution for a crack opened by a constant pressure σ_y°.* Then the solution to the outstanding three-dimensional problem in essence becomes a local free-surface correction to the two-dimensional problem. Formally the basic problem statement for the infinite geometry remains intact except that: the upper surface stress-free conditions (9) and the crack-face opening-pressure

*Indeed for the integral equation set ultimately constructed here, this removal is essential if the improper integrals involved are to converge.

conditions (10) become

$$\sigma_z = -\sigma_z^P,\ \tau_{yz} = \tau_{xz} = 0, \tag{29}$$

on $\partial_1 Q$ (σ_z^P as in (13)) and

$$\sigma_y = \tau_{xy} = \tau_{yz} = 0, \tag{30}$$

on $\partial_2 Q$ respectively, and the infinity conditions (12) are simplified with *all* the stresses now being $o(1)$.

To derive integral equations for this modified problem we seek to superimpose point loads on the quarter-space Q. Unfortunately no solutions expressed in elementary closed forms appear to exist for such point loads. Fortunately though, if we form the quarter-space as the intersection of two half-spaces (Fig. 5), we have at our disposal the Boussinesq solution for a normal point load on a half-space (the simple forms for which can be found in Timoshenko and Goodier [29], pp. 398-402). That is, we form Q as

$$\begin{aligned} Q &= H_1 \cap H_2, \\ H_i &= \{(x,y,z) \mid -\infty < x < \infty,\ -\infty < (i-1)y + (2-i)z < \infty, \\ &\qquad 0 < (2-i)y + (i-1)z < \infty\}\ (i=1,2), \end{aligned} \tag{31}$$

with corresponding surfaces $\partial_1 H$, $\partial_2 H$ given by

$$\begin{aligned} \partial_i H = \{(x,y,z) \mid &-\infty < x < \infty,\ -\infty < (i-1)y + (2-i)z < \infty, \\ &(2-i)y + (i-1)z = 0\}\ (i=1,2). \end{aligned} \tag{32}$$

Then the symmetric superposition of four equal point loads P at $x = \pm\alpha$, $z = \pm\beta$ on $\partial_1 H$ together with four equal point loads P' at $x = \pm\chi$, $y = \pm\psi$ on $\partial_2 H$ satisfies the field equations throughout Q and the zero shear stress conditions on $\partial_1 Q$, $\partial_2 Q$, $\partial_3 Q$, and reflects the last plane of symmetry, the yz-plane: it remains to distribute P,P' so as to satisfy $\sigma_z = -\sigma_z^P$ on $\partial_1 Q$, $\sigma_y = 0$ on $\partial_2 Q$, and $v = 0$ on $\partial_3 Q$. We now treat each of these in turn.

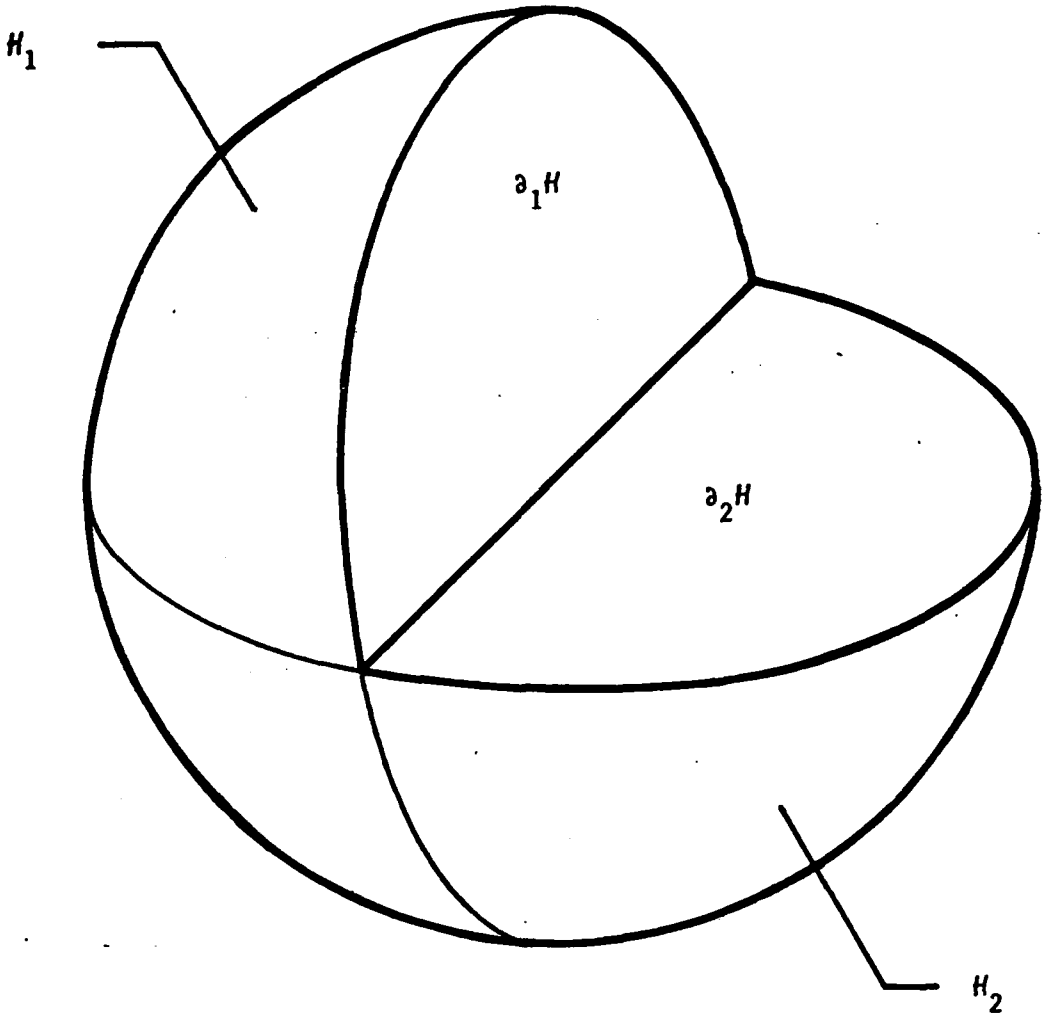

Figure 5. Intersection of two elastic half-spaces to form a quarter-space.

By superposition, the normal stress σ_z induced on the symmetry plane of H_1, $H_1 \cap \partial_2 H$, in response to four Boussinesq point loads of magnitude P symmetrically exerted at $x = \pm\alpha$, $z = \pm\beta$ on $\partial_1 H$ is

$$\sigma_z = PF(\alpha, \beta; x, y), \tag{33}$$

on $\partial_1 Q = H_1 \cap \partial_2 H$, where

$$F(\alpha,\beta;x,y) = \frac{1}{\pi} \sum_{i=1}^{2} [- 3\beta^2 y / R_i^5 + (1-2\nu)((y^2 + \beta^2)(y + 2R_i) - R_i^3)/(R_i^3 (y + R_i)^2)], \tag{34}$$

$$R_i = \sqrt{[(x + (-)^i\alpha)^2 + \beta^2 + y^2]} \quad (i = 1,2).$$

Hence if P is replaced by the loadette $p(\alpha,\beta)$ acting on the element $d\alpha d\beta$ centered on (α,β), and $p(\alpha,\beta)$ distributed throughout the quadrant $(0 < \alpha < \infty,\ 0 < \beta < \infty)$ we have

$$\sigma_z = \int_0^\infty\int p(\alpha,\beta)F(\alpha,\beta;x,y)d\alpha d\beta, \tag{35}$$

on $\partial_1 Q$. Since H_1 becomes H_2 on interchanging y and z, the stress σ_y induced on the symmetry plane at H_2, $H_2 \cap \partial_1 H$, in response to four point loads of magnitude P' at $x = \pm\chi, y = \pm\psi$ on $\partial_2 H$, is given by (33) with y interchanged with z, P replaced by P', and α,β by χ,ψ. It follows then that the response to loading $p'(\chi,\psi)$ distributed throughout $(0 < \chi < \infty,\ 0 < \psi < \infty)$ is:

$$\sigma_y = \int_0^\infty\int p'(\chi,\psi)F(\chi,\psi;x,z)d\chi d\psi, \tag{36}$$

on $\partial_2 Q \cup \partial_3 Q = H_2 \cap \partial_1 H$. Now combining the distribution p' on $\partial_2 H$ with the response to p there (35), satisfaction of the first of the outstanding requirements implies that

$$\sigma_z = -p'(x,y) + \int_0^\infty\int p(\alpha,\beta)F(\alpha,\beta;x,y)d\alpha d\beta = -\sigma_z^P, \tag{37}$$

on $\partial_1 Q$. Similarly satisfaction of the second implies

$$\sigma_y = -p(x,z) + \int_0^\infty\int p'(\chi,\psi)F(\chi,\psi;x,z)d\chi d\psi = 0, \tag{38}$$

on $\partial_2 Q$. Eliminating p' from (37), (38) gives the *stress integral equation*, our first integral equation for determining the unknown p,

$$p(x,z) - \int_0^\infty\int\left[\int_0^\infty\int p(\alpha,\beta)F(\alpha,\beta;\chi,\psi)d\alpha d\beta\right]F(\chi,\psi;x,z)d\chi d\psi = \int_0^\infty\int \sigma_z^P(\chi,\psi)F(\chi,\psi;x,z)d\chi d\psi, \tag{39}$$

on $\partial_2 Q$.

Turning to the last of the outstanding conditions to be met, the displacement condition, we observe that only the distributed loading p on $\partial_1 H$ contributes to the prescribed displacement component. To get this contribution we draw on the Boussinesq solution to assemble the displacement in the y-direction on the plane $H_2 \cap \partial_1 H$ in response to a set of four equal point loads at $x = \pm\alpha$, $z = \pm\beta$. Then the requirement that the response to the distribution p be zero yields the *displacement integral equation*, our second integral equation in the unknown p,

$$\int_0^\infty\int p(\alpha,\beta)f(\alpha,\beta;x,z)d\alpha d\beta = 0, \tag{40}$$

on $\partial_3 Q$, where

$$f(\alpha,\beta;x,z) = \frac{1-\nu}{2\pi\mu}\sum_{i=1}^{2}\sum_{j=1}^{2} 1/\sqrt{[(x + (-)^i\alpha)^2 + (z + (-)^j\beta)^2]}. \tag{41}$$

Equations (39), (40) constitute our fundamental set of Fredholm integral equations in the single unknown pressure p; in essence, they provide the local three-dimensional free-surface correction to the two-dimensional problem. Before moving on to their numerical solution, some comments on certain analytical aspects are in order.

Observe that σ_z^P is $O(1/(x^2 + y^2))$ on $\partial_1\Omega$ as $(x^2 + y^2) \to \infty$ and, since the decay of the Boussinesq stress-kernel is $O(1/(x^2 + y^2 + z^2))$ as $(x^2 + y^2 + z^2) \to \infty$, the decay of the unknown p can be inferred as $O(1/(x^2 + y^2))$ on $\partial_2\Omega \cup \partial_3\Omega$ as $(x^2 + y^2) \to \infty$; under these conditions the improper integrals in equations (39),(40) are guaranteed to be convergent. Note also that, when $\nu = 0$, σ_z^P of (13) is zero, which leads to p being zero in (39), (40) and the only known closed-form 3-D solution to (9)-(12) is recovered exactly - the instance where the three-dimensional solution becomes two-dimensional. Unfortunately equations (30), (40) appear resistant to the generation of further complete analytical solutions. Nonetheless, by making successive approximations on the unknown $p = p^{(n)}$, commencing with the trivial $p^{(o)} = 0$, and changing variables by setting $x-a = \rho\sin\theta$ and $z = \rho\cos\theta$, ρ being the distance from the crack vertex and θ the angle away from the crack front, we obtain

$$p^{(1)} = \frac{\Theta}{\sqrt{\rho}} . \tag{42}$$

Here Θ is a function of θ alone, not everywhere zero. Of course this asymptotic treatment is incomplete and in fact on continuing the substitution, contributions from the displacement equation may result in the cancellation of that in (41). At this time the complete analytical asymptotic analysis of (39),(40) is a subject of ongoing research, one on which we would welcome the assistance of other investigators.

In actuality the unknown pressure p is not the quantity of greatest physical import but rather the *energy release rate* that results from it. In order to obtain this crack driving energy G from p we proceed as follows. We represent G at a given depth z with Sanders' integral [36] in an xy-plane, take advantage of the symmetry of our configuration to restrict the contour of integration to one lying in the half-plane $y > 0$, then select the contour

as a quarter-circle ($x^2 + y^2 = R^2$, $x > 0$, $y > 0$) together with its radial ray on the y axis ($x = 0$, $0 < y < R$). Now, provided we include the plane strain solution for a crack opened under constant pressure together with a hydrostatic tensile field for an uncracked half-space (a field which leaves G itself unaltered), integrating by parts and invoking equilibrium results in the contribution from the circular portion of the contour vanishing as the radius of the quarter-circle tends to infinity ($R \to \infty$), leaving

$$G = \int_0^{\infty} \left(\sigma_x \frac{\partial u}{\partial x} + v \frac{\partial \tau_{yz}}{\partial z} - \sigma_y \frac{\partial v}{\partial y}\right) dy, \qquad (43)$$

on $x = 0$. To obtain the terms in the integral of (43) we take the plane strain and hydrostatic tensile fields as well as the stresses and displacements obtained by integrating the pressure distributions p, p' multiplied by the appropriate Boussinesq kernels over the surfaces $\partial_1 H$, $\partial_2 H$ respectively. We can then use (43) to evaluate the variations in G along the crack front when we assume a given crack-front shape; for a crack front to be *critical* though with a constant G we must solve the free-boundary problem described earlier. The adaptation of equations (39),(40) to accommodate such a crack-front search is straightforward and details may be found in [28].

The integral equations for assessing the effects of presumed *residual compressive stresses* can also be easily derived, essentially by following the same procedure as for the basic infinite 3-D problem. That is, after subtracting the plane strain problem to ensure convergence, superposition of point loads to satisfy the outstanding boundary conditions yields integral equations identical to the basic problem except equation (39) is altered by adding σ_y^r of (19) to its right-hand side.

For any of these preceding integral equation sets our approach to their *numerical* solution is a simple one - a *collocation procedure*. In sum this

entails taking due account of the expected singular behavior of the unknown, transforming it so as to admit representation as a piecewise constant on subregions of the boundary, and thereafter specializing the integral equations to hold at the centroids of these discretization regions to generate a square linear algebraic system of equations with integral coefficients for the determination of the unknown.

To implement the procedure we first *nondimensionalize* the integral equations by dividing the coordinates x,z and variables of integration α,β,χ,ψ by the semi-crack length a (or $\lim_{z\to\infty} a(z)$ in the event of a free boundary problem), and the stress σ_z^p (and σ_y^r for a residual stress problem) and the unknown pressure p by the crack opening pressure σ_y°, denoting all the quantities so formed by their original symbols with a bar atop.

To *regularize* the new unknown $\bar{p}$ it is only necessary that we remove an overestimate of its singular character. Recalling our earlier discussion in the introduction it would seem likely that this could be achieved in the basic problem by introducing a square-root singularity and accordingly we do this here by setting

$$\bar{p} = \frac{\bar{x}\,\bar{q}}{\sqrt{(\bar{x}^2-1)}} \quad (\bar{x} > 1), \tag{44}$$

where $\bar{q}$ is the new "regular" unknown and the particular way in which the square-root singularity is introduced in (44) is in anticipation of a subsequent change of variable to remove it. In addition, from our previous remark that the decay of p is $O(1/(x^2 + z^2))$ as $(x^2 + z^2) \to \infty$ we require, away from the origin, a further transformation on $\bar{p}$ to reflect this decay and ensure convergence and so take

$$\bar{p} = \frac{\bar{x}\,\bar{q}}{(\bar{x}^2 + \bar{z}^2)\sqrt{(\bar{x}^2-1)}} \quad (\bar{x}^2 + \bar{z}^2 \gg 1). \tag{45}$$

Of course we cannot guarantee that $\bar{q}$ of (44),(45) is indeed continuous and should a stronger singularity participate at the crack vertex it would not be; though we expect this is not the case, the vindication of the regularization in (44), (45) ultimately rests with the numerical results found using it. In contrast we do expect $\bar{q}$ not to be continuously differentiable at the crack vertex so that any discrete representation other than a *piecewise constant* would not appear warranted. With this representation, the discretization of the surfaces $\partial_2 Q$, $\partial_3 Q$ on which $\bar{q}$ is represented proceeds as follows.

Unlike most boundary integral methods the surfaces on which our equations hold are not of finite extent. As a result, the initial division of the boundary, $\partial_2 Q \cup \partial_3 Q$, is into *finite regions* S and *infinite regions* I. For our preliminary discretization *grid* or *map*, the limits of the finite regions are chosen to enclose the area having more than one percent variation from the normal stress component σ_y of the plane strain solution as estimated by the previous numerical analyses of Cruse and Van Buren [24] and Tan and Fenner [25]. Inside the border of this region the grid is refined near the free surface and crack front to capture the expected behavior in the unknown $\bar{q}$. A solution to this system is found for an initial grid and the element-to-element variation in $\bar{q}$ used as an indication of how the grid can be rearranged/extended so as to smooth and model variations. This partially optimized mesh is then systematically refined to study convergence on a sequence of grids comprised of a coarse (31 boundary elements), a medium (109), and a fine (421). To indicate the maximum resolution the fine grid is shown in Fig. 6.*

The only remaining numerical issue is the *quadrature* to be used to

*Refer Burton [37] for a fuller account of the discretization process.

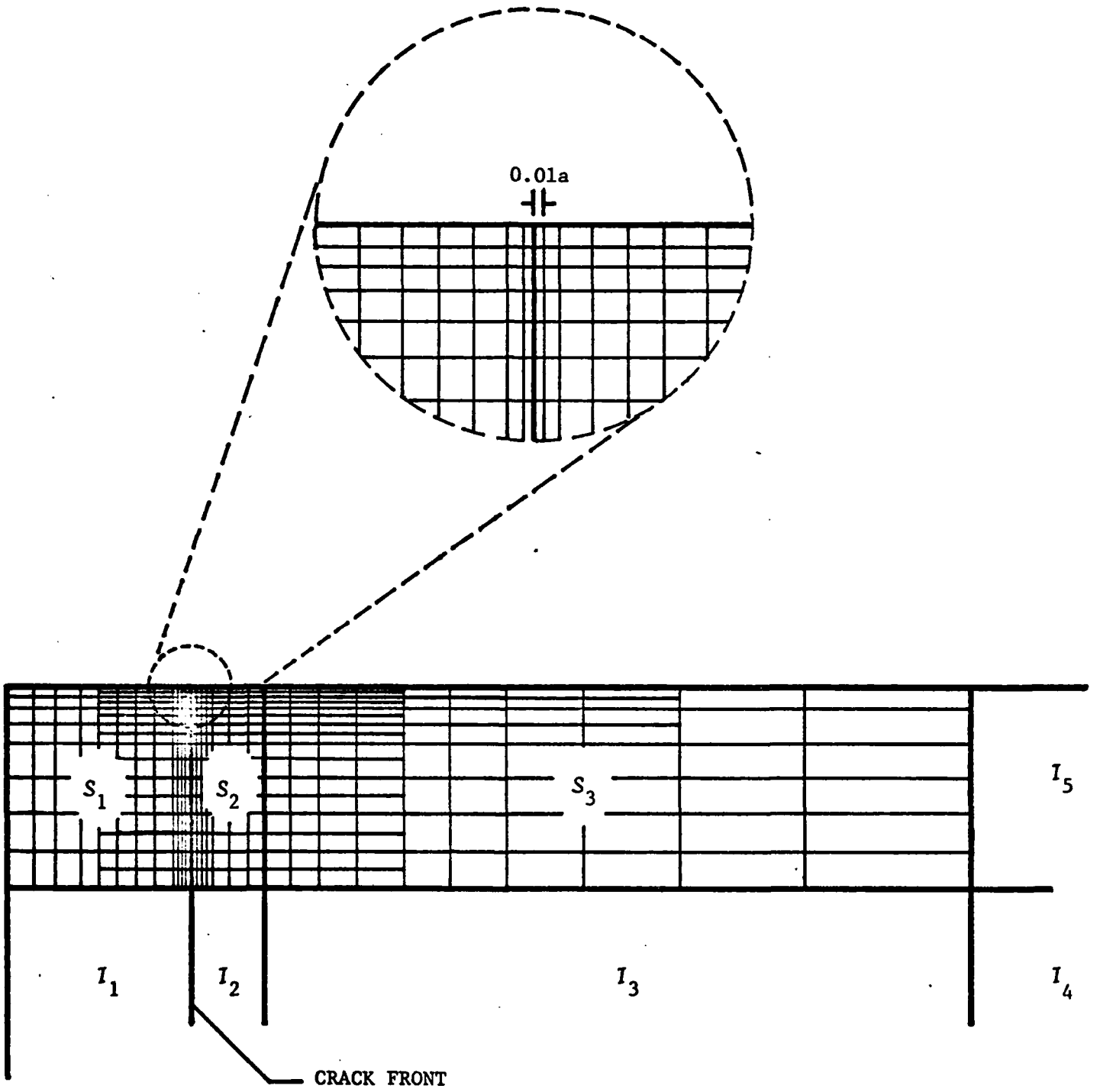

Figure 6. Fine discretization of the plane for the integral equations.

determine the matrix coefficients in the linear set of equations. This quadrature must recognize the singular or near-singular behavior of the Boussinesq response kernels as well as the singularity introduced through (44), (45), the latter becoming smooth away from the crack front ($\bar{x} > 1$). Thus, to simplify the integration, no transformation is used away from $\bar{x} \to 1^+$. In Fig. 6 subdomains of S, S_i (i = 1-3), and I, I_i (i = 1-5), are shown and represent to scale the sections where the following respective transformations are used: 1, $\bar{x}/\sqrt{(\bar{x}^2 - 1)}$, 1; $1/\bar{z}^2$, $\bar{x}/(\bar{z}^2\sqrt{(\bar{x}^2-1)})$, $1/\bar{z}^2$, $1/(\bar{x}^2 + \bar{z}^2)$, $1/\bar{x}^2$. A consequence of selectively transforming the unknown is that the quadrature on S_1, S_3, which together comprise the greater part of S, merely entails determining the response of an elastic half-space to a constant pressure applied over a rectangle on its surface. Hence Love's solution [38] can be used to perform this integration exactly. The quadrature on the remainder of S, the surface S_2 wherein the transformation (44) is applied, is undertaken using an adaptation of the first mean value theorem which recognizes the singularity introduced via (44). The quadrature on the infinite surfaces is less important since the grid itself is designed so that the unknown values associated with these regions are practically negligible, *i.e.*, so that the key results should be left virtually unchanged if we set these integrals to zero. With this in mind, the only singularity directly handled is that occurring on I_2 as a result of the transformation there, the approach being the advertised change of variable, specifically $\bar{x}' = \sqrt{(\bar{x}^2-1)}$. Thereafter all of the infinite surfaces are mapped into finite ones and a mid-point rule employed - a rule generally consistent with the approximation underlying our discretization. For those few instances when the untreated inverse-distance singularity in the Boussinesq displacement kernel makes its present felt, the quadrature is confirmed simply by applying the mid-point rule on successively smaller quadrature

intervals.*

With all of these aspects of the procedure in place the numerical solution becomes routine since, although the coefficient matrix is neither symmetric nor sparse, it is well-conditioned and quite amenable to reduction by standard Gaussian elimination. While the computational effort required is not great for the resolution gained,** the results found directly are limited to a single stress component in the crack plane and even for this one quantity cannot reasonably be expected to quantify its singular character very accurately. Thus it is in part in order to overcome these shortcomings, as well as to provide a verifying comparison, we next turn to our finite element analysis.

To facilitate grid gradation our finite element approach employs two types of regular or host elements which are mutually compatible: an eight-node isoparametric hexahedron or brick, and a six-node isoparametric pentahedron or wedge formed by coalescing two node-pairs in the brick element (Figs. 7A, B). In natural coordinates (ξ,η,ζ) the displacements u are represented by the following interpolation functions

$$u = c_1 + c_2\xi + c_3\eta + c_4\zeta + c_5\xi\eta + c_6\eta\zeta + c_7\xi\zeta + c_8\xi\eta\zeta, \qquad (46)$$

$$u = c_1 + c_2\xi + c_3\zeta + c_4(1+\xi)\eta + c_5\xi\zeta + c_6(1+\xi)\eta\zeta,$$

*Again more detail can be found in Burton [37].

**The central processing times on the time-sharing DEC-20 system at Carnegie-Mellon being of the order of 1 minute, 20 minutes and 3 hours for the coarse medium and fine grids respectively, with matrix reduction consuming only $\sim$8 minutes of the fine grid time.

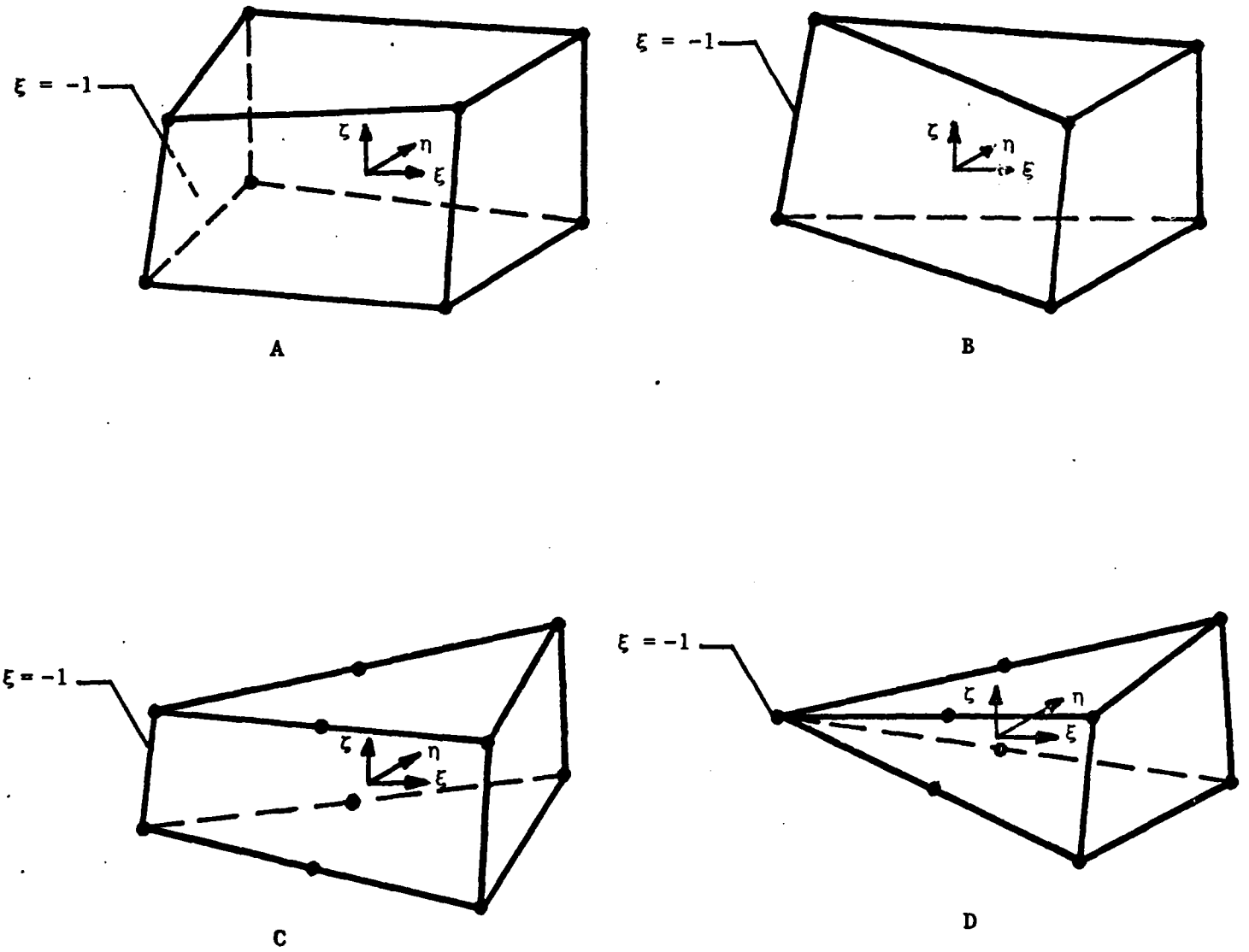

Figure 7. Elements for the FEM analysis: A-regular hexahedron, B-regular pentahedron, C-singular pentahedron, D-singular tetrahedron.

where c_i (i = 1-8) are vectors of constants, readily expressed in terms of nodal values of u.* Being isoparametric the respective coordinate transformations share the same representations as in (46).

The class of crack problems at hand also requires two basic types of *singular element*, one with a line singularity for the crack front, the other with a point singularity for the crack vertex. We construct these singular elements after Tracey [39] by inserting mid-side nodes in a regular element and letting the additional degrees of freedom model the desired singular behavior. The advantages of this method of development are that a singular element so formed retains its constant stress and strain capabilities while maintaining full interelement displacement continuity with non-singular elements. On the negative side, the coordinate transformations remain those of the original regular element so that a singular element's edges must be kept straight with the extra nodes fixed at their midpoints in real (x,y,z) space, a subparametric element therefore. Nevertheless, provided we abide by these restrictions, such singular elements would seem to be among the best for present purposes.

In detail we proceed as follows. We form a ten-node pentahedron from the regular pentahedron (Fig. 7c) and use the extra degrees of freedom to represent the inverse square-root singularity expected at the crack front away from the upper surface. Hence for this element

$$u = c_1 + c_2\xi + c_3\zeta + c_4(1+\xi)\eta + c_5\xi\zeta + c_6(1+\xi)\eta\zeta$$

$$+ c_7(1-\zeta)\sqrt{(1+\xi)} + c_8(1+\zeta)\sqrt{(1+\xi)} + c_9(1-\zeta)\eta\sqrt{(1+\xi)} + c_{10}(1+\zeta)\eta\sqrt{(1+\xi)}. \tag{47}$$

We then collapse the two nodes on the line singularity into one to provide

*To avoid the introduction of a number of distinguishing notations, the one nomenclature c_i is used in (46) and future interpolation functions even though such c_i are in general different.

a nine-node tetrahedron or pyramid (Fig. 7d) and free up the singular nature by taking

$$u = c_1 + c_2\xi + c_3(1+\xi)\eta + c_4(1+\xi)\zeta + c_5(1+\xi)\eta\zeta$$
$$+ c_6(1+\xi)^{1-\lambda} + c_7\eta(1+\xi)^{1-\lambda} + c_8\zeta(1+\xi)^{1-\lambda} + c_9\eta\zeta(1+\xi)^{1-\lambda}, \tag{48}$$

with λ continuing its role as a singularity exponent. The corresponding singular stress behavior generated by (47), (48) is then

$$\sigma = O(1/\sqrt{r}) \text{ as } r \to 0, \ \sigma = O(1/\rho^{\lambda}) \text{ as } \rho \to 0, \tag{49}$$

r, ρ being as in our initial coordinate system (Fig. 1).*

To determine the *singularity exponent* we adopt the procedure in Swedlow [15] wherein λ becomes an additional parameter to aid in minimizing potential energy. Of course this minimization seeks the lowest potential energy possible using the limited representations available in the singular element and thus may elect to model some part of the regular local fields that is not perfectly captured by the constant strain terms with a little of the λ-singularity fields: given the different natures of the two fields, such eigenfunction smearing is not seen as a major impediment to the evaluation of λ using minimization but it does serve as a warning not to expect tremendous resolution in such determinations in complete problems that have quite a number of different local fields excited.

The *quadrature* required for the minimization is performed using Gauss rules, with *singular* Gauss rules for the singular elements. The actual schemes used are extensions to 3-D of the two-dimensional singular rule

*To ensure compatibility between the displacements of (47), (48) we actually need a further element with a line singularity, a transition element wherein the $\sqrt{(1+\xi)}$ in the c_8, c_{10} terms is replaced by $(1+\xi)^{1-\lambda}$ - refer Solecki [40] for greater detail.

used by Stern [41]. These extensions are simple in concept but somewhat algebraically complex because of the higher-order dimension - a full description is given in Solecki and Swedlow [42].

With the representations, minimization procedure, and quadrature in place it remains to apply our finite element method to the class of problems of concern here. As a result of some numerical experimentation, the element map selected for the baseline problem is as shown in Fig. 8 and has 375 elements including 49 line-type singular elements and 7 point-type, 1587 degrees of freedom all told, and similar resolution to the medium grid in the integral equation analysis.* Perturbations of this map also serve to investigate curved critical crack profiles. As is characteristic of FEM, the attendant calculations provide a wealth of information concerning the field quantities throughout the plate from which it is straightforward to calculate energy release rates using a path independent integral such as the J integral (Rice [43]). Alternatively these key quantities can be calculated using the more computationally convenient device of virtual crack extension (as in Parks [44]), provided care is exercised in controlling truncation errors. The results of such calculations together with those from the integral equation analysis are considered next.

4. Verification: LEFM implications of results

Here we discuss those calculations which serve to validate our twin analyses starting with checks on the integral equation treatment, then comparing integral equation results with finite element, and finally looking at

*CPU times for this grid are of the order of 1 hour compared to 20 minutes for the medium grid in the integral equation approach on the same computing system.

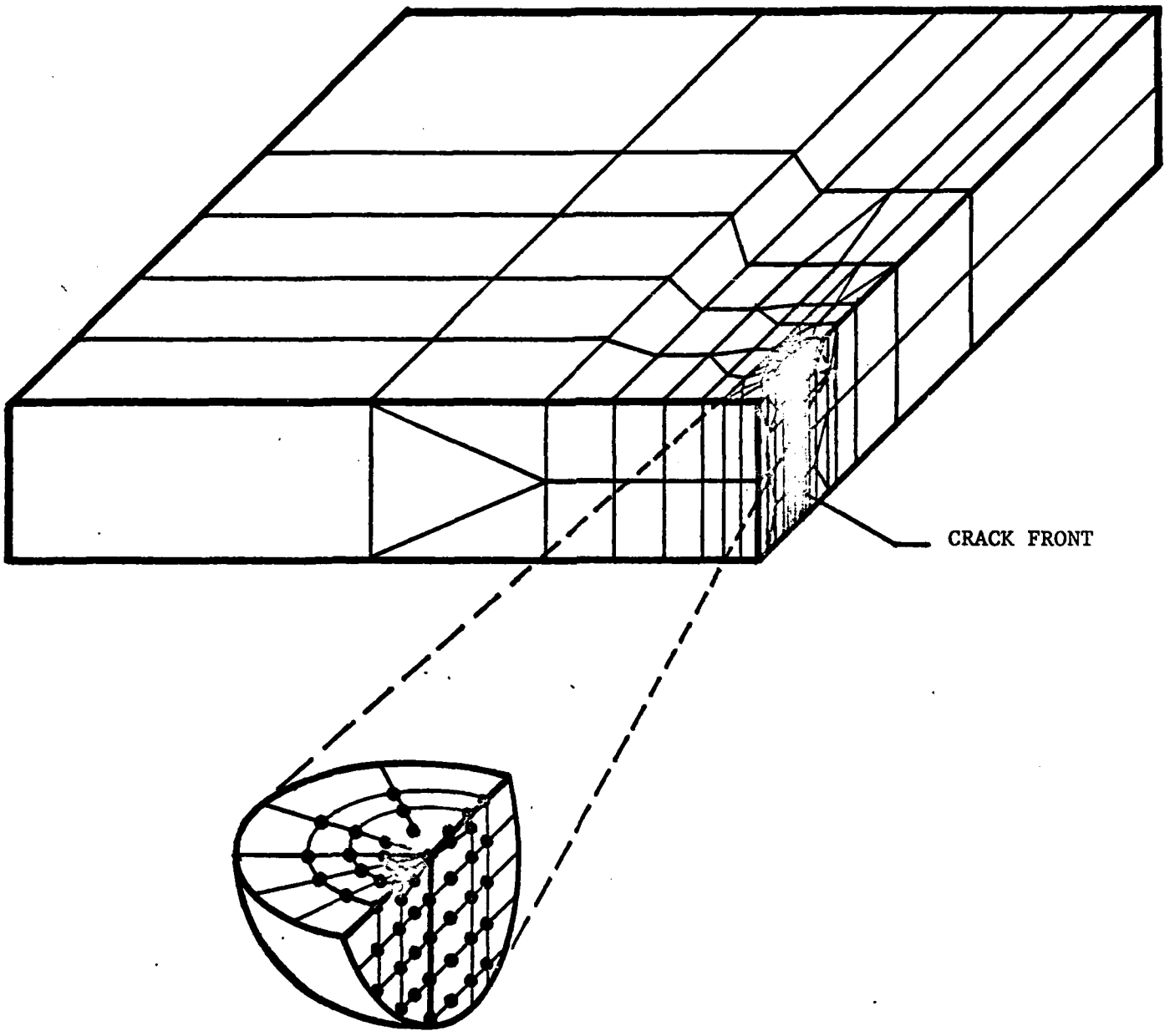

Figure 8. Grid for the FEM analysis of the plate octant.

other means of confirming the FEM analysis. With the resolution of the two approaches calibrated we close the section by considering selected results which address the issues raised earlier and are obtained from whichever method is deemed most advantageous computationally.

A first point of corroboration of our integral equation approach is found in the magnitudes of the three-dimensional correction away from the crack, namely the values of the unknown p on the infinite surfaces I_i(i=1-5). These p-values at the collocation points on I_i are uniformly less than 2% of σ_y°, thereby vindicating our choice of the extent of the finite regions in the discretization and supporting the justification advanced in Section 3 for performing the quadrature in the infinite regions with a simpler but less refined scheme than in the finite. A second point of corroboration lies in the estimates of the "regular" unknown $\bar{q}$ which are indeed numerically consistent with a continuous unknown and, in particular, exhibit no evidence of a stronger singularity at the crack vertex than that removed by the transformations (44), (45), if anything indicating the opposite. These numerical results therefore add credence to our expectation concerning singular behavior expressed at the outset and also suggest that the numerical values of the unknown determined via the integral equations should converge well.

To examine convergence we consider the unknown pressure p by itself rather than the complete stress solution including the plane strain response, since it is for this quantity alone that convergence is of primary importance. Further we confine attention to the region nearest the crack front since this is the region wherein p's role is most significant. Fig. 9 shows coarse, medium and fine grid determinations of dimensionless pressure p/σ_y° as a function of depth z/a at the closest distance from the crack front

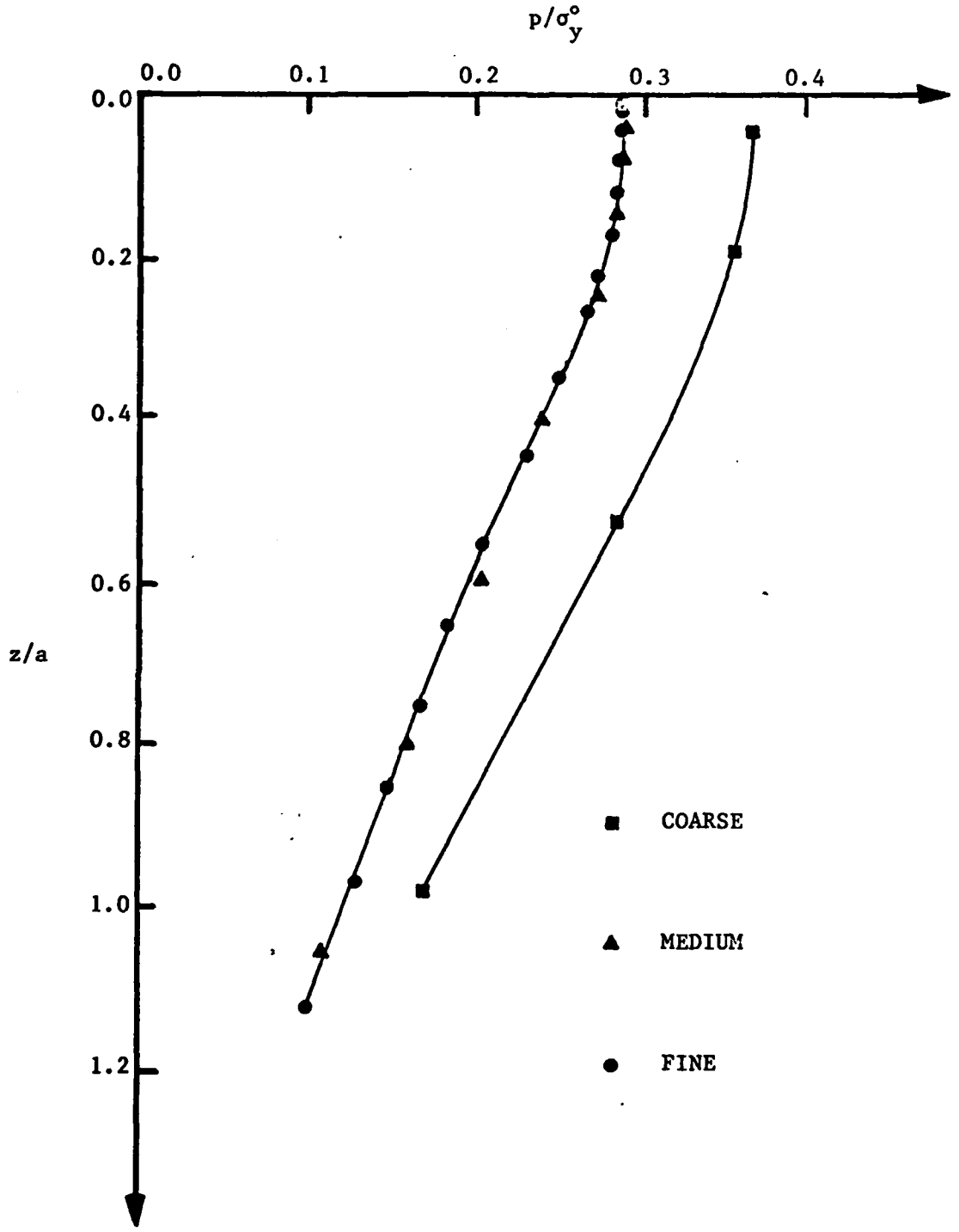

Figure 9. Convergence of integral eguation unknown p of closest common station ahead of the crack (x/a = 1.05, υ = 0.3).

common to all three grids, $x/a = 1.05$, and for Poisson's ratio $\nu = 0.3$. The curves in Fig. 9 are consistent with a numerically convergent procedure, the results for the medium and fine grids being almost indistinguishable on the scale that space permits in the figure.

As the finite element analysis is less amenable, in terms of computational effort, to the further refinement necessary to establish convergence, we choose instead to infer this quality by comparison with integral equation results, again focusing on the critical region near the crack front.* We do this by taking the complete normal out-of-plane stress in the crack plane from the integral equation results in conjunction with the same stress component from the plane strain solution for a crack under *far-field applied tension*, and comparing the stress so assembled with the corresponding response computed using finite elements on plates whose plate thicknesses are increased until the mid-plate answers are within 3% of the integral equation results at the same location (the actual thickness thus found being $h/a = 2$). The results as functions of depth z/a at the two lines of centroids closest to the crack front available from the FEM, $x/a = 1.05$, 1.14, and for $\nu = 0.3$, are shown in Fig. 10 and represent good agreement given the gradients present (*cf.* for example, the different numerical results for the same configuration in Raju and Newman [19], p. 34). Accordingly it would appear that the finite element results from the grid of Fig. 8 are convergent.

Other ratifications of the FEM analysis are the perfect response to a patch test, so confirming the interelement compatibility claimed, and the evaluation of the energy release rate in a two-dimensional test

*In this connection observe that halving element sides to form a more refined grid, the procedure in essence adopted for the integral equations, would lead to an FEM map of around 3000 elements and 13000 degrees of freedom.

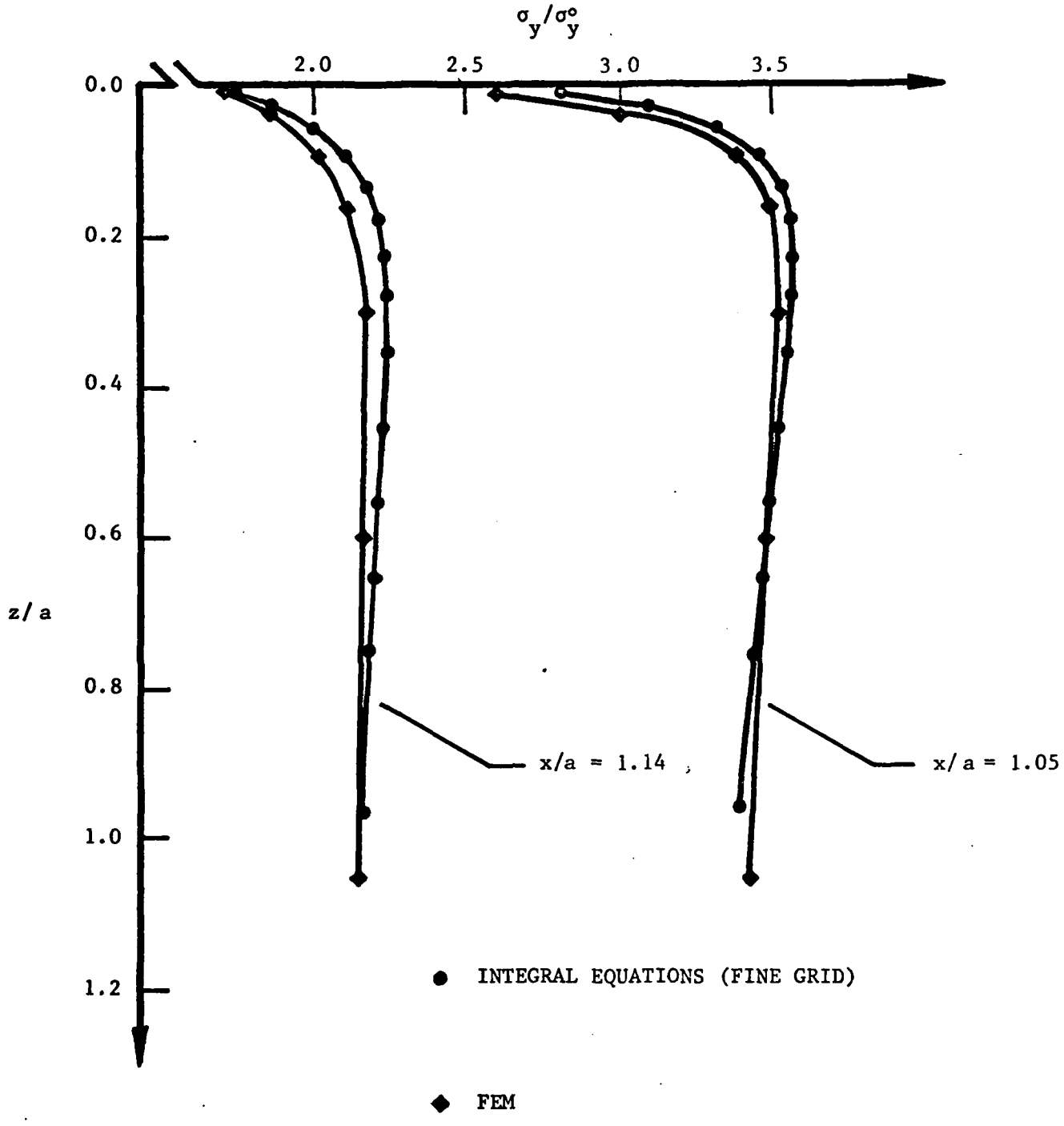

Figure 10. Comparison of integral equation and FEM results for the normal stress ahead of the crack ($\upsilon = 0.3$).

problem to within 0.1% using the element arrangement of Fig. 8 and the J integral. Though not strictly a verification because of the different physics actually present and that theoretically assumed, an experimental comparison with the holographic interferometry study of Limtragool [45] affords an additional appraisal of the resolution of our FEM procedure. Fig. 11 displays w, the displacement in the direction of the crack front at the crack vertex (see Fig. 1 for local geometry, Limtragool [45], p. 63 for full specimen geometry), as a function of y, the surface distance transverse to the crack, for high-strength Aluminum Alloy 6061-T6 ($\mu = 26 \times 10^3$ MPa, $\nu = 0.33$), both as found experimentally and via an analysis of the actual specimen geometry using our finite element capability. The agreement shown is not as good as for the same displacment component's variation with the other surface distance x (Limtragool [45] p. 89) but is nontheless remarkable. Also presented in Fig. 11 is an approximate two-dimensional estimate as determined from simple integration of the out-of-plane strain in a plane stress analysis: the discrepancy between this last and the physical response emphasizes the inherent three-dimensionality of the displacement plotted in Fig. 11.

With our two approaches checked we now consider the implications of their results within the context of linear elastic fracture mechanics, beginning with the initial step in LEFM, the identification of singular nature.* For this activity, only the finite element approach can be reasonably used and the results found using it for the adjustable singularity exponent λ of (48), (49) as a function of Poisson's ratio ν are summarized in Table 1, together with those of other researchers.

*More comprehensive results than those reported here may be found in Burton [37] and Solecki [46] for the integral equation and finite element investigations respectively.

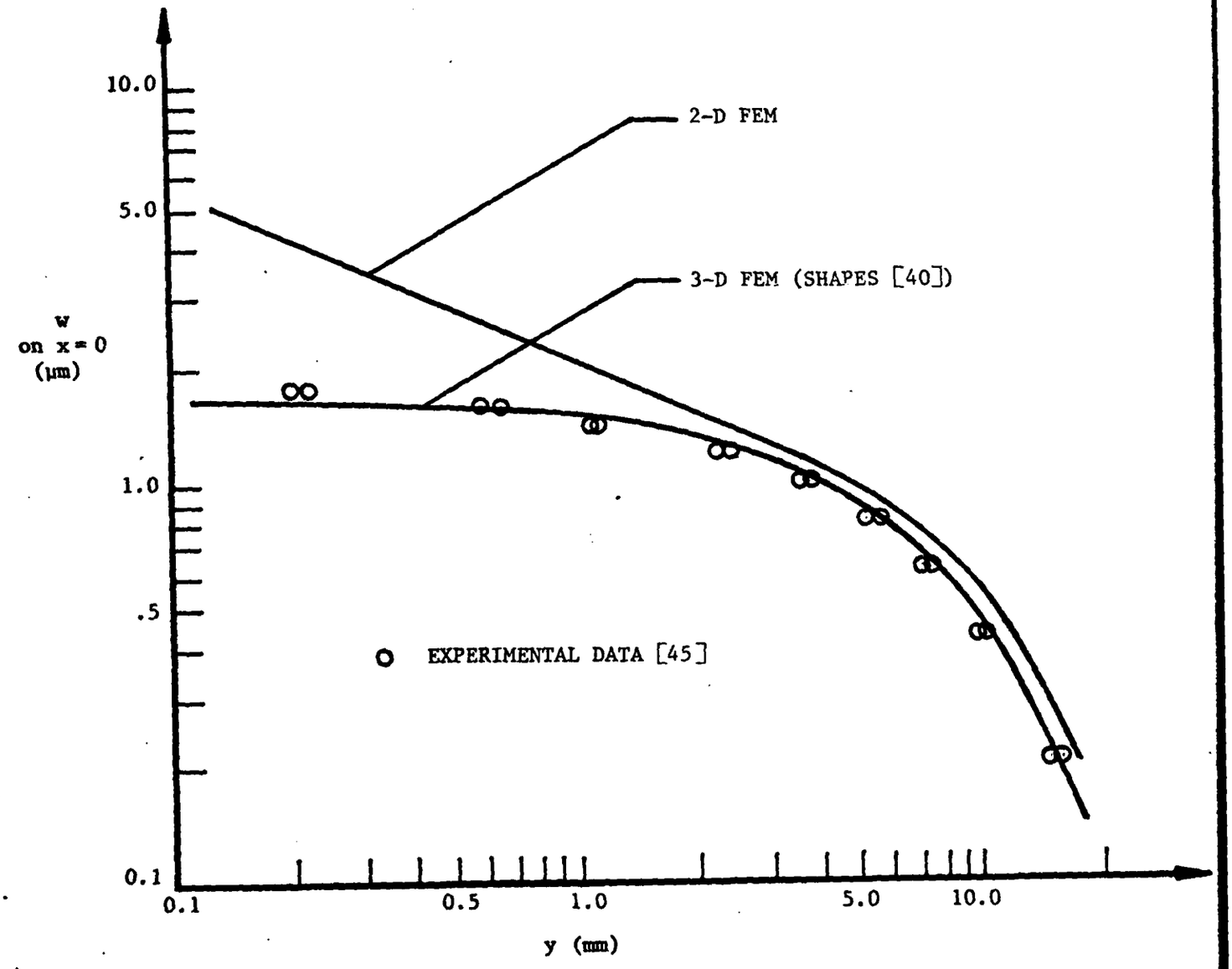

Figure 11. Comparison of FEM and experimental results for the normal displacement on the free surface (Limtragool [45]).

TABLE 1

Singularity exponent at the crack vertex (λ in $\sigma = O(1/\rho^{\lambda})$)

Source	$\nu = 0.0$	$\nu = 0.15$	$\nu = 0.3$	$\nu = 0.4$
Analytical by Benthem [5]	0.500	0.484	0.452	0.413
Analytical by Kawai *et al.* [6]	0.50	0.48	0.43	0.37
Finite difference by Benthem [11]	0.500	0.484	0.452	0.414
FEM by Bažant & Estenssoro [12]	0.500	0.484	0.452	0.413
FEM by present treatment	0.499	0.485	0.445	0.370

The results in Table 1 from our analysis are for a plate with h/a = 1, there no longer being a need to simulate the infinite half-space and a less distorted grid being preferred. An indication of a probable upper limit on the resolution of our results is given by the λ-value for $\nu = 0$ which is 0.001 in error from the known exact result of 1/2. In view of their likely resolution for other ν they should not be interpreted as supporting the cited λ-values of Kawai *et al.* [6] over those of Benthem's analysis [5], but rather as being in general agreement with both, no evidence of the stronger singularity of [6] being found in our specific configuration. In contrast, the close agreement of the numerical work of Benthem [11] and Bažant and Estenssoro [12] with Benthem's analytical values [5] does support the last over the corresponding ones in Kawai *et al.* [6] by virtue of the fact that [11], [12] treat problems especially tuned to λ-determination

instead of the global problems analyzed here.* The import of all the results in Table 1 is that the energy release rate should be zero right in the upper surface for normal crack intersection when $\nu \neq 0$ and, given a continuous variation along the crack front, that G should decay near the surface in this instance. We investigate this proposition next.

As argued previously these energy release rates are to be determined in planes parallel to the free surface. The method favored as being the most reliable for this determination is by means of path independent integrals in such planes. Since the FEM analysis yields the information needed in such evaluations more readily than the integral equation approach, we use the finite element results to this end here. Specifically we again take $h/a = 1$ and use the J integral (after Rice [43]) as well as virtual crack extension (after Parks [44]) to compute G, the former serving to check the more computationally convenient latter. In instances in which both methods of G-determination are applied the same results are obtained for all practical purposes, justifying the use of the second method for intervening results. These results as functions of depth for various Poisson's ratios are given in Fig. 12, with G therein being normalized by its plane strain value G_p. *Mathematically* the indications are that G should be identically zero in the free surface for $\nu \neq 0$ but that it can be non-zero arbitrarily close to the free surface: *numerically* we find a decay of G as the free surface is approached ($z/a \to 0$) with the largest drop between the maximum value and that of the closest Gauss point to the free surface occurring, as expected, when ν takes on the maximum value considered (0.4), and being 30% of G_p.

The configuration analyzed to provide the results in Fig. 12 does not

*Regards comparing the present finite element analysis with that of Bažant and Estenssoro [12], it is worth noting that [12] has the highly comparable results of $\lambda = 0.485$ for $\nu = 0$ and $\lambda = 0.380$ for $\nu = 0.4$ on the fine grid therein prior to exploiting convergence to extrapolate, an option not open to us here.

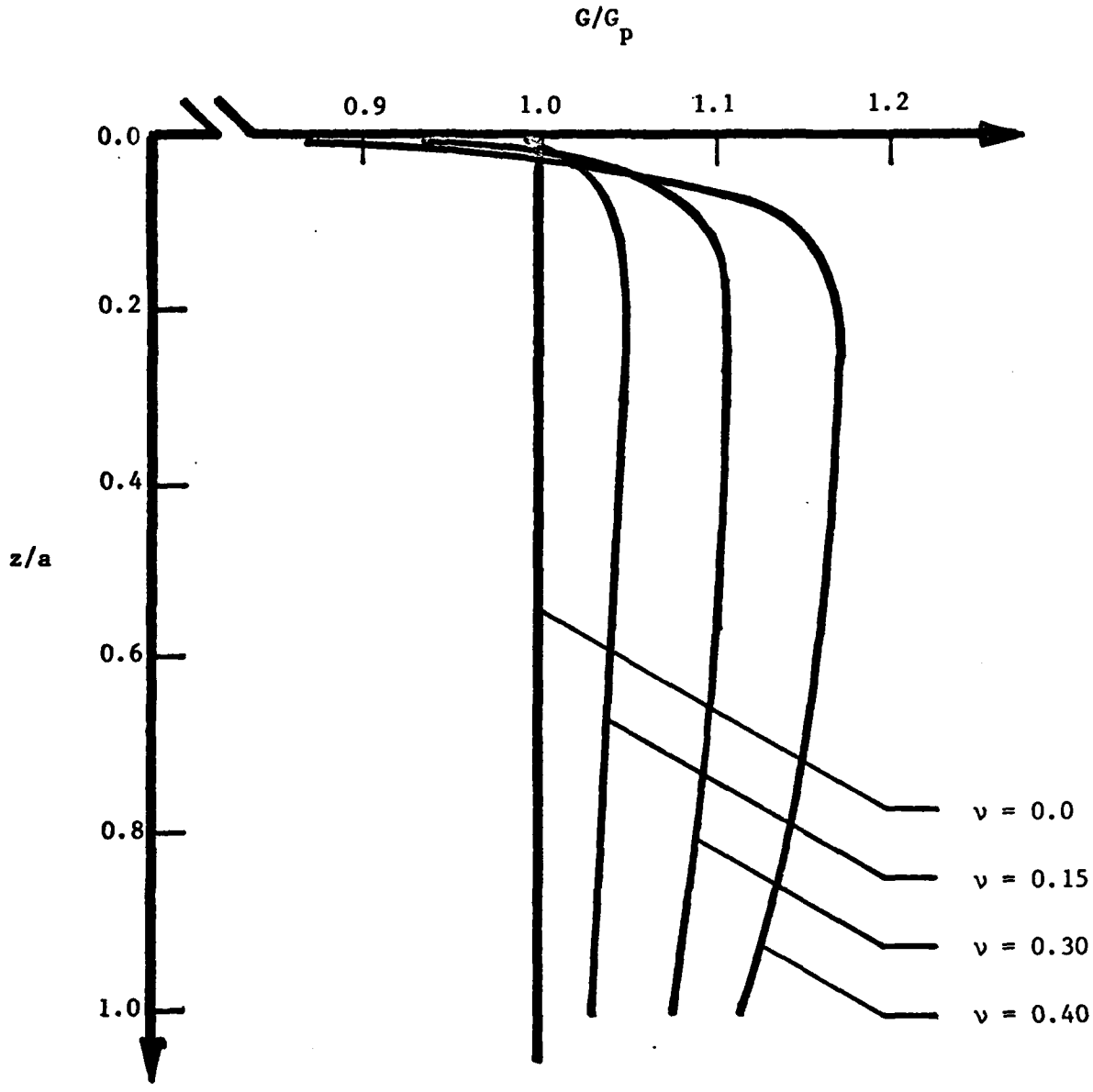

Figure 12. Decay of the energy release rate at the free surface for normal intersection (h/a = 1).

coincide with any of the standard specimens used in the determination of the critical energy release rate G_c, *i.e.*, in fracture toughness testing (see [47]). Nonetheless it is somewhat similar in that it entails opening or Mode I excitation and in that $h/a = 1$ is the nominal ratio prescribed for all of the standard test pieces in [47]. Accordingly we can infer what inaccuracies are introduced in standard toughness tests as a result of not accounting for three-dimensional variations with the two-dimensional plane strain value. From Fig. 12 we see that, if indeed the crack front is perfectly straight as assumed in the standards [47], then the G_c calculated from a two-dimensional analysis of a test could be as much as 18% less than the real material value for $\nu = 0.4$ and typically would range from 4-12% smaller (corresponding conservative errors in the critical value of the stress intensity factor K_c being 9% for high ν with a normal range of 2-6 %).* Given the overall scatter usually encountered in fracture toughness testing, these sorts of error are not out of line.

In the cyclic life estimation component of LEFM the import of the results of Fig. 12 are less clear. Ignoring three-dimensional effects and assuming a single $\Delta\sqrt{G(\Delta K)}$ for a through crack in a plate in a cyclic life calculation is certainly not completely correct, but since the test data used in such calculations is usually analyzed with the *same* simplifying assumption the errors introduced by the pair of simplifications would appear to compensate in large part. Of course, 3-D LEFM implies that for $\nu \neq 0$ the straight profiles associated with the varying Gs of Fig. 12 would not propagate as such but rather take up curved profiles with constant energy release rates: we next investigate what shapes these crack fronts must adopt in order to compensate for the drop-offs in G displayed in Fig. 12.

*These statements presume that the specimen would in fact fracture when the three-simensional maximum G attained the critical material value G_c for unstable crack propagation, then taking the G-value calculated from two-dimensional analysis at that load as G_c gives rise to the lower values indicated.

In view of the free surface reductions in energy release rate it would seem reasonable to advance the crack front away from the upper surface so as to undercut the material ahead of the crack near the surface thereby increasing the energy release rate there and approaching a constant G profile. Indeed the physical evidence suggests this is the case (as in, say, Bell and Feeney [33]) and Bažant and Estenssoro [12] theoretically determine a crack/surface intersection angle which deviates from perpendicular in a manner consistent with subsurface crack advance and which strengthens the vertex singularity to the point of enabling a nontrivial G to exist right in the free surface. Accordingly we look for critical crack fronts of this type here, beginning our search by treating moderate ν-values because we know the answer for $\nu = 0$ is simply the straight crack with normal intersection. In this way the critical profiles of Fig. 13 are generated for succesively larger values of Poisson's ratio, each profile shown therein having less than a 2% numerical variation in G with depth z/a. These results illustrate that only a minor amount of crack front curvature is needed to render a profile critical in an LEFM sense, the greatest deviation from straight occurring for the maximum ν of 0.4 and representing an advance of less than 2% of the semi-crack length a: that is, a 30% variation in G is overcome by an order of magnitude less change in crack-front profile.

The implications of these results regarding critical G determination or fracture toughness testing are as follows. Logically LEFM requires that, if toughness testing is to take into account three-dimensionality, the governing test specifications should admit limited two-sided deviations in actual specimen crack fronts about *curved profiles* that are everywhere critical like those of Fig. 13. As it happens, present standards [47] already do this since they permit a considerable curvature and, moreover, the allowable scatter is such that the most curved of the present profiles for

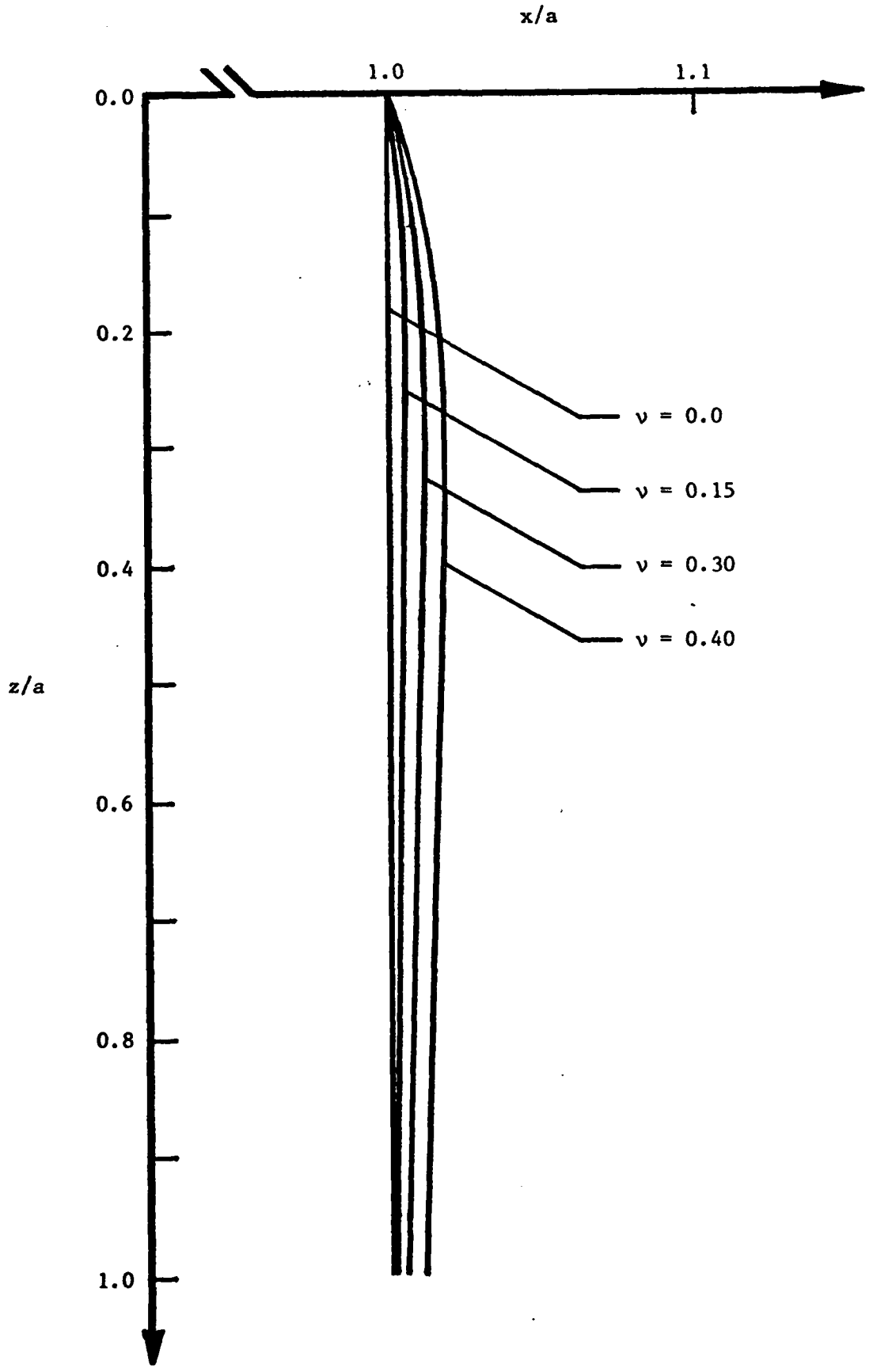

Figure 13. Critical crack profiles possessing constant energy release rates (h/a = 1)

$\nu = 0.4$ is placed well within this spread. Indeed, in reflecting large amounts of testing experience, the most recent standards [47] allow far greater curvature than the most curved profile in Fig. 13, possibly because of the presence of some shallow, surface, residual, compressive stresses. Without quantification of such fields, an accurate assessment as to the appropriateness of the standards in this regard is impossible, but subsequent results reported here do indicate that the increased curvature permitted in [47] is qualitatively reasonable.

Implications for cyclic crack growth calculations in LEFM are less easily arrived at. While it is clear that only minor modifications in crack front shape are necessary to produce the sort of profile which undergoes self-similar growth - an implicit assumption in much of current two-dimensional cyclic life estimation - it is not so obvious how to simply adjust two-dimensional calculations to account for the overall three-dimensional increase (here about 10%) in G, hence $\Delta\sqrt{G}$. As mentioned earlier, provided these increases are comparable in the calibrating test and the application, their effects should cancel to some extent. However in instances wherein there are significant differences between the two situations it is possible that significant losses of accuracy could accrue. One possible type of fundamental difference between a data generating test specimen and the configuration to which it is applied is in relative thickness and we consider this effect next.

Fig. 14 presents FEM results for energy release rates normalized with respect to the plane strain value as functions of depth for $\nu = 0.3$ and the two finite thickness extremes treated here, the fattest being that used to simulate the basic infinite geometry and having $h/a = 2$, the thinnest having $h/a = 0.3$. The variation in G increases as thickness decreases with the change from maximum to minimum going from 11% of G_p when $h/a = 2$ to 20%

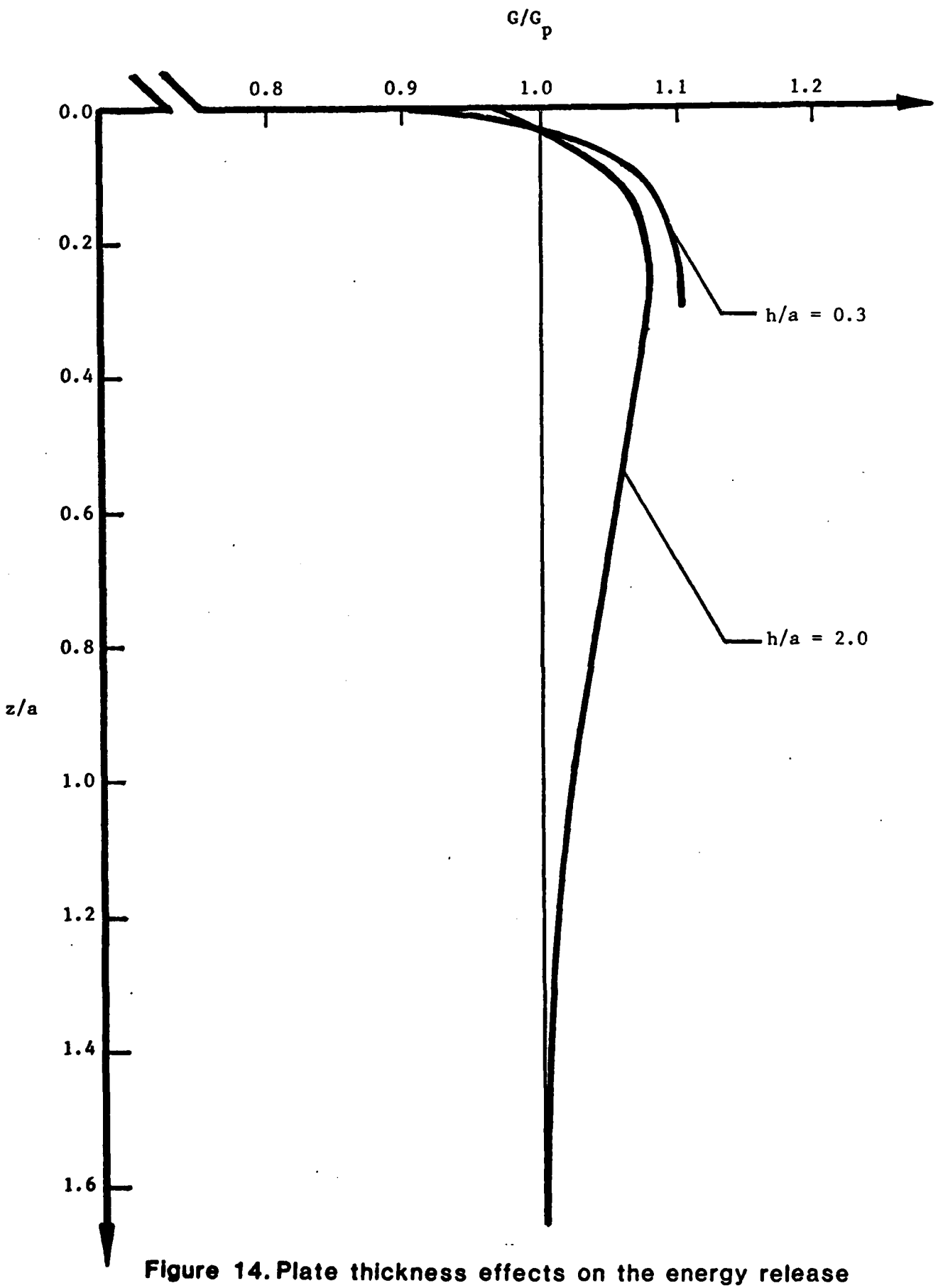

Figure 14. Plate thickness effects on the energy release rates for normal intersection ($\upsilon = 0.3$).

of G_p when h/a = 0.3. This trend may explain in part the disagreement between the integral equation and finite element results in Fig. 10 since it is possible that the FEM results there showed a somewhat greater free-surface reduction due to finite thickness effects, *viz*, the possibility that h/a = 2 does not completely simulate an infinite half-space. On the other hand the value of G in Fig. 14 at maximum depth for h/a = 2 would seem to support the contention that this thickness of plate is close to "infinite".

While the drop-off in G changes in Fig. 14, the average value is increased by less than 3% as plate width reduces - well within the 10% increase predicted in two-dimensions for $\nu = 0.3$ as one goes from plane strain to plane stress - and the excess of G over the two-dimensional value (G_p) remains nearly constant. Consequently little error would seem to be introduced in two-dimensional cyclic life calculations from ignoring three-dimensional *elastic* effects when the test specimen differs markedly from the application geometry in thickness.

A further 3-D factor possibly affecting cyclic life calculations are residual stresses and Fig. 15 shows the effect on the energy release rates of the following presumed residual stress fields: *superficial* with σ_y^r decaying to 1% of σ_y° at z/a = 0.05 (γ = 92.1 in (19)), *shallow* with decay depth z/a = 0.3 (γ = 15.4), *medium* with decay depth z/a = 0.6 (γ = 7.7), and *deep* with decay depth z/a = 1.2 (γ = 3.8). These results are readily calculated using the integral equation approach since we can now check a local stress-fitting determination of G - the easiest for the integral equation results - with a more reliable finite element calculation using a path independent integral. This check for the instance of no residual stress gives the attendant energy release rate G_o to within 1%. Normalizing the other energy release rates in the presence of residual stresses G_r by G_o, we see in Fig. 15 that sizable reductions in energy release rate occur in the presence of residual compressive stresses, both at the surface and at

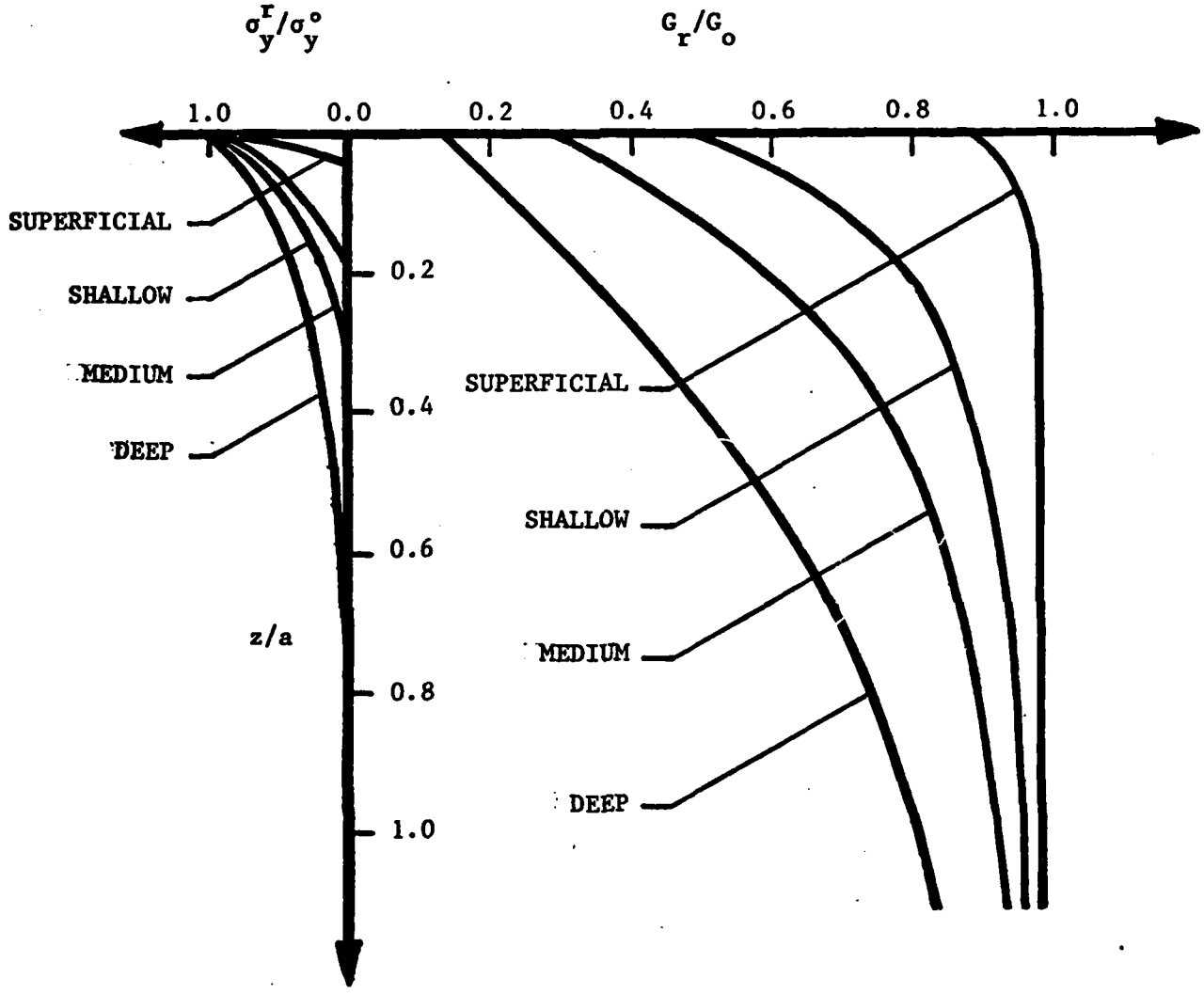

Figure 15. Presumed compressive residual stresses and resultant relative energy release rates for normal intersection ($\upsilon = 0.3$).

depths considerably greater than the decay depths of the corresponding residual stress field - clearly a three-dimensional effect and not something that one would readily estimate from any approximate two-dimensional analysis. While these calculations are for *hypothetical, presumed,* residual, stress fields they do serve notice of the potentially major impact of residual stresses on cyclic life calculations even within LEFM, and the need to quantify such fields therefore if better cyclic life estimates are to be determined.

5. Concluding remarks

The consensus emerging from the literature of a weaker singularity at a normal crack/surface intersection in analyses of local problems is further supported by the present investigation of some global crack/surface intersection problems. A degree of confidence in the present results can be gained from the good agreement of two independent numerical analyses and the performance of these two approaches with respect to a number of checks. The two methods also provide information on the key quantity in linear elastic fracture mechanics, the energy release rate, for a variety of configurations from which the following conclusions may be drawn.

The three-dimensional implications of crack/surface intersections regarding fracture toughness testing may reasonably be disregarded as it would appear they can be in most present day cyclic life calculations. One exception to this last, however, may well be in near-surface residual stress effects and the idealized pilot study presented here indicates a need to understand such fields better. In sum, but for residual stress effects, it would seem unlikely that any results of great practical consequence would be furnished from the further study of elastic crack/surface intersection problems. This is not to say there are not some important three-dimensional elastic crack problems to be considered. Indeed, the apparent paradox of cyclic crack growth at $\Delta\sqrt{G}$ levels for which the maximum Gs attained are less

than G_c strongly suggests that this problem is three-dimensional, with portions of the crack front departing from a simple straight profile and as a result experiencing energy release rates in excess of G_c: some credibility is lent to this possiblity by the present investigation since the rearrangements to obtain critical crack fronts may be reinterpreted as indicating that small changes in crack profiles can lead to far larger variations in G, whence $\Delta\sqrt{G}$. Used with sufficient care the sort of methods developed here may be able to investigate this suggestion and, if successful, could lead to a physically reasoned explanation of fatigue crack growth - certainly an understanding which is potentially of major practical significance.

Acknowledgements

We would like to thank H.E. Donely and G.T. Fix of the Mathematics Department at Carnegie-Mellon University for their helpful suggestions and advice, especially regarding the numerical solution of the integral equations. The financial support of the Air Force Office of Scientific Research under grant number AFOSR-79-0078 is also appreciated.

References

[1] V.V. Panasyuk, A.E. Andrejkiv and M.M. Stadnik, *Engineering Fracture Mechanics* 13 (1980) 925-937.

[2] V.V. Panasyuk, A.E. Andrejkiv and M.M. Stadnik, *Engineering Fracture Mechanics* 14 (1981) 245-260.

[3] O.K. Aksentian, *Journal of Applied Mathematics and Mechanics (Prikladnaia Mathematika i Mekhanika)* 31 (1967) 193-202.

[4] M.L. Williams, *Journal of Applied Mechanics* 19 (1952) 526-528.

[5] J.P. Benthem, *International Journal of Solids and Structures* 13 (1977) 479-492.

[6] T. Kawai, Y. Fujitoni and K. Kumagai, *Proceedings of the International Conference on Fracture Mechanics and Technology* (Hong Kong) (1977) 1157-1163.

[7] G.B. Sinclair, *Proceedings of the Seventh Canadian Congress of Applied Mechanics* (Sherbrooke, Quebec), 1 (1979) 295-296.

[8] R.D. Gregory, *Journal of Elasticity* 9 (1979) 283-309.

[9] E.S. Folias, *Journal of Applied Mechanics* 42 (1975) 663-674.

[10] J.P. Benthem and W.T. Koiter (discussion), E.S. Folias (closure), *Journal of Applied Mechanics* 43 (1976) 374-375.

[11] J.P. Benthem, *International Journal of Solids and Structures* 16 (1980) 119-130.

[12] Z.P. Bažant and L.F. Estenssoro, *International Journal of Solids and Structures* 15 (1979) 405-426, 16 (1980) 479-481.

[13] Z.P. Bažant, *International Journal of Engineering Science* 12 (1974) 221-243.

[14] J.L. Swedlow, Development of the program SPECEL, a special element for elasto-plastic crack-tip stress analysis, Report SM 74-10, Department of Mechanical Engineering, Carnegie-Mellon University, Pittsburgh (1974).

[15] J.L. Swedlow, *International Journal for Numerical Methods in Engineering* 12 (1978) 1779-1798.

[16] Y. Yamamoto and Y. Sumi, *International Journal of Fracture* 14 (1978) 17-38.

[17] G. Yagawa and T. Nishioka, *International Journal for Numerical Methods in Engineering* 12 (1978) 1295-1310.

[18] G. Yagawa and T. Nishioka, *International Journal of Solids and Structures* 16 (1980).

[19] I.S. Raju and J.C. Newman, Three-dimensional finite-element analysis of finite-thickness fracture specimens, NASA Technical Note D-8414, National Aeronautics and Space Administration, Washington (1977).

[20] M.F.O. de Sebra Pereira, Three-dimensional linear-elastic fracture mechanics analysis of thick-walled pressure vessel components, D. Phil. Dissertation, Imperial College of Science and Technology (1977).

[21] A.A. Tseng, *Engineering Fracture Mechanics* 13 (1980) 939-943.

[22] P.D. Hilton and B.V. Kiefer, *Journal of Pressure Vessel Technology* 102 (1980) 347-352.

[23] J.P. Gyekenyesi and A. Mendelson, *International Journal of Fracture Mechanics* 11 (1975) 409-429.

[24] T.A. Cruse and W. Van Buren, *International Journal of Fracture Mechanics* 7 (1971) 1-15.

[25] C.L. Tan and R.T. Fenner, *Proceedings of the Royal Society* (London), A369 (1979) 243-260.

[26] E.S. Folias, *International Journal of Fracture* 16 (1980) 335-348.

[27] B.I. Smetanin and B.V. Sobol, *Journal of Applied Mathematics and Mechanics (Prikladnaia Matematika i Mekhanika)* 45 (1981) 707-709.

[28] G.B. Sinclair, Derivation of the integral equations for the three-dimensional crack problem, Report SM 79-10, Department of Mechanical Engineering, Carnegie-Mellon University, Pittsburgh (1979).

[29] S.P. Timoshenko and J.N. Goodier, *Theory of Elasticity* (Third Edition), McGraw-Hill, New York (1970).

[30] A.E. Green and W. Zerna, *Theoretical Elasticity* (Second Edition), Oxford at the Clarendon Press (1968).

[31] G.R. Irwin, *Journal of Applied Mechanics* 24 (1957) 361-364.

[32] J.G. Kaufman, in *Developments in Fracture Mechanics Test Methods Standardization*, ASTM Special Technical Publication 632, Philadelphia (1976) 3-24.

[33] P.D. Bell and W.J. Feeney, Fractographic evaluation of fracture specimens, Technical Report AFFDL-TR-75-152, Grumman Aerospace Corporation, Bethpage, New York (1976).

[34] J.O. Almen and P.H. Black, *Residual Stresses and Fatigue in Metals*, McGraw-Hill, New York (1963).

[35] M. Isida, *International Journal of Fracture Mechanics* 7 (1971) 301-316.

[36] J.L. Sanders, *Journal of Applied Mechanics* 27 (1960) 352-353.

[37] W.S. Burton, Some inherently three-dimensional problems in linear elastic fracture mechanics, Ph.D. Dissertation, Carnegie-Mellon University (1983).

[38] A.E.H. Love, *Transactions of the Royal Society* (London) A228 (1929) 377-420.

[39] D.M. Tracey, *Nuclear Engineering and Design* 26 (1974) 282-290.

[40] J.S. Solecki, SHAPES - A Finite Element Program for the Analysis of Elastic Three-Dimensional Cracks, Report SM 81-12, Department of Mechanical Engineering, Carnegie-Mellon University, Pittsburgh (1981).

[41] M. Stern, *International Journal for Numerical Methods in Engineering* 14 (1979) 409-421.

[42] J.S. Solecki and J.L. Swedlow, *International Journal for Numerical Methods in Engineering*, in press.

[43] J.R. Rice, *Journal of Applied Mechanics* 35 (1968) 379-386.

[44] D.M. Parks, *International Jou nal of Fracture* 10 (1974) 487-502.

[45] J. Limtragool, Investigation of the three-dimensional behavior of a crack tip singularity by holographic interferometry, Ph.D. Dissertation, Carnegie-Mellon University (1982).

[46] J.S. Solecki, Three-dimensional elastic analysis of straight and curved through cracks in plates of finite thickness, Ph.D. Dissertation, Carnegie-Mellon University (1983).

[47] E399-81 Standard test method for plane-strain fracture toughness of metallic materials, *1982 Annual Book of ASTM Standards*, American Society for Testing and Materials, Philadelphia (1982) 592-622.

List of related publications/presentations

Journal publications

G.J. Fix, M.D. Gunzburger and R.A. Nicholaides, On mixed finite element methods for first order elliptic systems, *Numerische Mathematik* 37 (1981) 29-48.

J. Solecki and J.L. Swedlow, On quadrature and singular finite elements, *International Journal for Numerical Methods in Engineering*, in press.

W.S. Burton, G.B. Sinclair, J.S. Solecki and J.L. Swedlow, On the implications for LEFM of the three-dimensional aspects in some crack/surface intersection problems, *International Journal of Fracture*, submitted.

Conference publications

G.B. Sinclair, Asymptotic singular eigenfunctions for the three-dimensional crack, *Proceedings of the Seventh Canadian Congress of Applied Mechanics* (Sherbrooke, Quebec), 1 (1974) 295-296.

W.S. Burton and G.B. Sinclair, On the 3-D implications of LEFM: I - An integral equation approach, *Sixteenth National Symposium on Fracture Mechanics* (Columbus, Ohio), accepted for presentation.

J.S. Solecki and J.L. Swedlow, On the 3-D implications of LEFM: II - Finite element analysis of straight and curved through cracks in a plate, *Sixteenth National Symposium on Fracture Mechanics* (Columbus, Ohio), accepted for presentation.

Doctoral dissertations

H.E. Donley, Finite element approximations to integral equations, Ph.D. Dissertation, Department of Mathematics, Carnegie-Mellon University (1981).

J.S. Solecki, Three-dimensional elastic analysis of straight and curved through cracks in plates of finite thickness, Ph.D. Dissertation, Department of Mechanical Engineering, Carnegie-Mellon University, in preparation.

W.S. Burton, Some inherently three-dimensional problems in linear elastic fracture mechanics, Department of Mechanical Engineering, Carnegie-Mellon University, in preparation.

Reports

The following independent reports have been written:

Report Numbers SM 78-18, SM 79-10, SM 79-20, SM 80-10, SM 81-12, SM 81-16 and SM 81-17, all issued by the Department of Mechanical Engineering, Carnegie-Mellon University (and all placed on file with AFOSR).

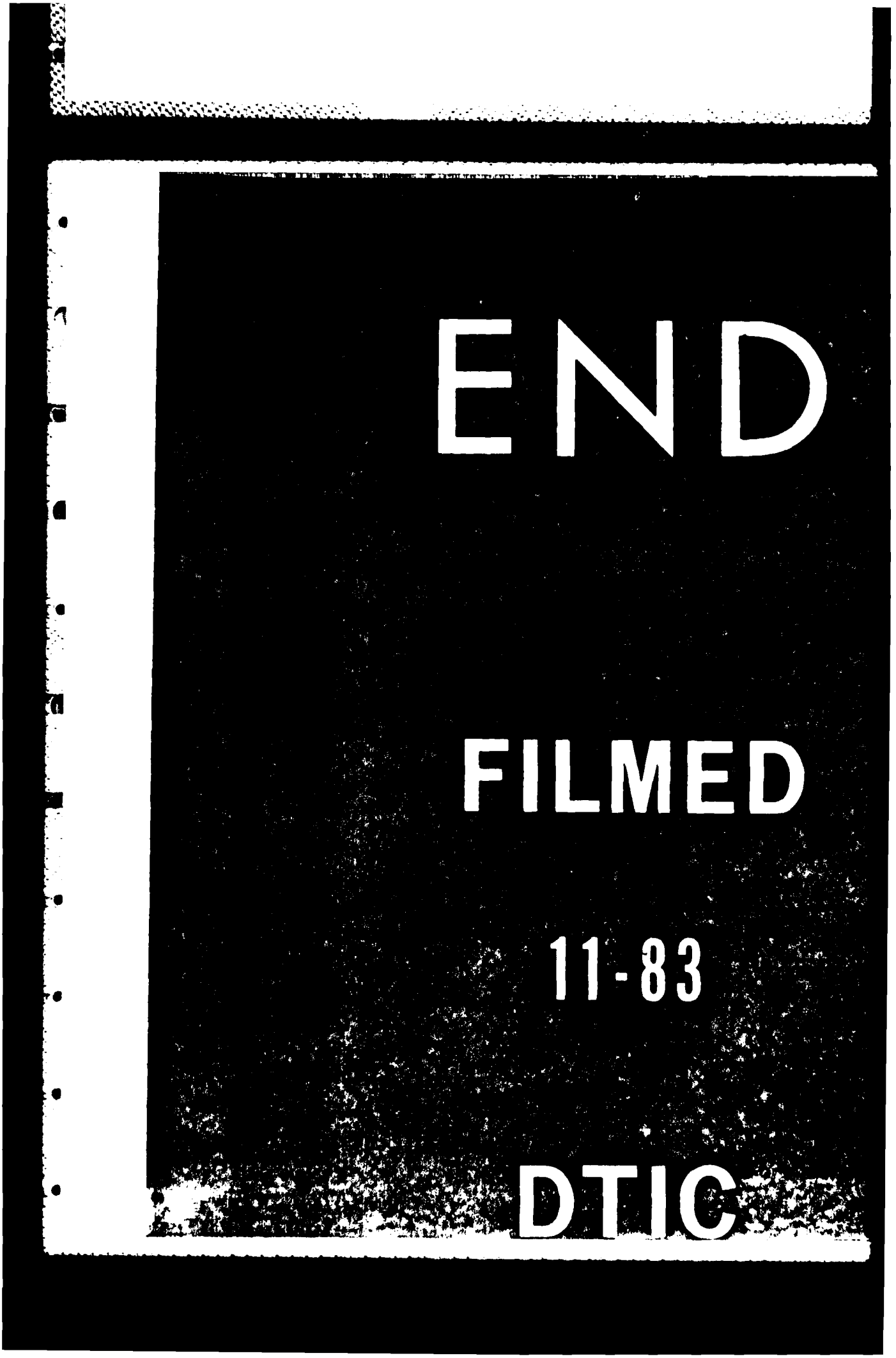
END
FILMED
11-83
DTIC